NOTICE: This is the author's version of a work that was accepted for publication in **NeuroImage**. Changes resulting from the publishing process, such as peer review, editing, corrections, structural formatting, and other quality control mechanisms, may not be reflected in this document. Changes may have been made to this work since it was submitted for publication. A definitive version was subsequently published in **NeuroImage**, Volume 98, September 2014, DOI: http://dx.doi.org/10.1016/j.neuroimage.2014.04.053

Please cite as:

Zanon M., Novembre G., Zangrando N., Chittaro L., Silani G. Brain activity and prosocial behavior in a simulated life-threatening situation, *NeuroImage, 98,* 2014, pp. 134-146

Brain Activity and Prosocial Behaviour in a Simulated Life-Threatening Situation

Marco Zanon[a*], Giovanni Novembre[a], Nicola Zangrando[b], Luca Chittaro[b] and Giorgia Silani[a]

[a]Cognitive Neuroscience Sector, International School for Advanced Studies, ISAS-SISSA, Via Bonomea 265, 34136 Trieste, Italy
[b]Human-Computer Interaction Lab (HCI Lab), Department of Mathematics and Computer Science, University of Udine, Via delle Scienze 206, 33100 Udine, Italy

*Corresponding author: Marco Zanon, Cognitive Neuroscience Sector, International School for Advanced Studies, SISSA- ISAS, Via Bonomea 265, 34136 Trieste, Italy. *E-mail*: mzanon@sissa.it

Abstract

To study the neuronal basis of altruistic behavior, we investigated functional connectivity within brain networks of participants who exhibited either a self-benefit behavior or an altruistic one in a life-threatening situation simulated in a virtual environment. In particular, participants were asked to evacuate a virtual building on fire and, without being previously informed, they were faced with a decision on whether to stop and help a trapped virtual human, at the possible cost of losing their own life in the virtual experience. Group independent component analysis (gICA) applied on blood-oxygen-level-dependent (BOLD) functional images revealed significant differences between the group of participants who showed selfish behavior and those who acted prosocially. Specifically, an increased functional connectivity in the salience network, comprising the anterior insula (AI) and the anterior mid cingulate cortex (aMCC), was observed in the selfish group compared to the prosocial one. Conversely, higher ICA weights in the medial prefrontal cortex and temporo-parietal junction (TPJ), were observed in the prosocial group. The findings show that an increased functional connectivity of the salience network, which suggests an enhanced sensitivity to the threatening situation and potential danger for the individual, resulted in more selfish choices, while the engagement of the medial prefrontal and temporo-parietal cortices subserved prosocial behavior, possibly due to their role in perspective-taking. The study provides the first online neurophysiological measurement of prosocial decision-making during threatening situations, opening new avenues to the investigation of neuronal substrates of complex social behaviors.

Keywords: prosocial behavior, virtual reality, gICA, salience network, mPFC.

1 Introduction

Contemporary human societies show the highest levels of complexity and social relationships, compared to any other animal species. Even if it is still a puzzle for many social scientists, such a complexity seems to be the driving force that has favoured the evolution of a larger and more complex brain (Byrne and Bates, 2007; Dunbar and Shultz, 2007; Silk, 2007). During evolution, humans have developed neuronal circuits dedicated to mental abilities that are fundamental to tie social bonds and effective interactions. Specifically, empathy, mentalizing and the capacity to understand other's actions are considered the basis of social cognition, (see Frith and Singer, 2008; Singer, 2012). Furthermore, evolution has promoted moral systems as well as cooperative and caring behaviors that go beyond relatedness and genetic similarities (Boyd, 2006; Fehr and Fischbacher, 2003). It has been recently proposed that intergroup competition and reproductive leveling might have allowed the proliferation of a genetically transmitted predisposition to behave altruistically (Bowles, 2006), i.e. engaging in actions that increase the benefits of other individuals, even if at our own costs. Despite the importance of this social phenomenon, the understanding of its neurophysiological basis is far from being complete (Lieberman, 2012; Singer, 2012), and some questions are greatly unsolved, such as why altruistic actions are so differently engaged among individuals and which cognitive and neurophysiological mechanisms are predictive of such behaviors.

In social neuroscience, the investigation of prosociality, fairness and altruism has taken advantage mainly of socio-economic games and other paradigms in which participants were asked to decide monetary allocation between themselves and another person (Rilling et al., 2002) or spontaneously donate a certain amount of their income (Waytz et al., 2012; FeldmanHall et al., 2012a; Morishima et al., 2012). However, altruistic behaviors do not always imply exclusively monetary losses in order to increase the welfare of another person, but also actions that could involve physical threat to the agent and, in the most extreme case, pose a risk to the agent's own life. Because of obvious experimental and ethical consideration, most of neuroscience studies investigating helping behaviors under physical threat have used scenarios with very limited ecological validity, such those described by a text or cartoon strips. As a result, it is difficult to transfer experimental findings to real-life contexts. FeldmanHall and collaborators have recently taken into account the effect of contextual information on participants' altruistic behavior (FeldmanHall et al., 2012a; FeldmanHall et al., 2012b). To investigate the gap between moral judgment and moral action, they observed that the amount of information available to the participants influences their choices in a 'Pain vs. Gain' paradigm. In particular, the more abstract the context, and the higher the need of mentalizing, the bigger is the gap between beliefs of acting altruistically and real behaviors. This study focused specifically on moral decisions, but demonstrated the difference between judgments and actions and that very limited scenarios may not accurately reflect social behaviours in everyday life. It therefore pinpointed the importance of ecologically valid and action-relevant experimental paradigms for testing complex behaviors such as moral cognition and prosocial behaviors (FeldmanHall et al., 2012b).

So far, only few studies have used real-life paradigms suitable for addressing the question of altruistic behavior under physical threat. An example is provided by Hein and colleagues who observed physiological and behavioral responses of participants who were given the possibility to prevent another person from suffering from physical pain, by 'sacrificing' themselves as the target of the painful stimulation. They showed that the strength of empathy-related skin conductance responses predicts later costly helping (Hein et al., 2011). Similarly, the authors provided evidence that activity in brain areas involved in empathy, such as the anterior insula, predicts the costly helping behavior later in time (Hein et al., 2010). Moreover, they observed that participants helped more frequently other participants considered as ingroup members, rather than outgroup members, and thus demonstrated that social context can influence prosocial decision-making.

In the present study, we aimed at extending the knowledge about the neurophysiology of prosocial decision making, by combining Virtual Reality (VR) with Independent Component

Analysis (ICA) of fMRI data. In particular, we used VR to simulate a life-threatening situation, in which participants were faced with the decision whether to save another participant, risking their own life. The employed methodology allowed us to avoid two main shortcomings in social neuroscience: on one hand, we were able to provide a contextually rich environment that the experimenter can control, without the obvious practical and ethical constraints of the classical experimental paradigms (Bohil et al., 2011); on the other hand, we were able to decode brain activity during a flowing experience, when no a priori models of signal changes are available (Beckmann, 2012; Spiers and Maguire, 2007; McKeown et al., 1998; Bressler and Menon, 2010; Guye et al., 2008).

Since the first studies that applied ICA as a model-free approach to fMRI data, it has been demonstrated that segregated patterns of neuronal activity can be consistently identified and that these intrinsic connectivity networks (ICNs) are present both at rest or during task performance (Arbabshirani et al., 2012; Beckmann, 2012; Bressler and Menon, 2010; Damoiseaux et al., 2006). Typically, ICNs include primary sensory and motor cortices, the default-mode network and attentive networks. It has been suggested that they represent functional networks, spatially segregated by the fact that they are differentially recruited according to the type of ongoing mental process (Cole et al., 2010).

By comparing neuronal activity between participants who showed a prosocial or a selfish behavior, we aimed at identifying the cognitive processes involved in social decision during a life-threatening situation. We hypothesized that the main differences among the groups would be observed in the salience network (Bressler and Menon, 2010; Seeley et al., 2007) and in the anterior part of the default-mode network (Uddin et al., 2009; Harrison et al., 2008a). The former comprises the anterior insula and the anterior cingulate cortex, two cortical areas involved in social cognition, empathy and prosocial behavior (Bernhardt and Singer, 2012), the later is constituted by the medial prefrontal cortex, a key brain region for social cognition (Mitchell et al., 2005; Bzdok et al., 2013).

2 Method

2.1 Participants

Forty-three healthy young adults (30 women, 13 men, M_{age}: 22,8, age range: 21-30 years, all right-handed) participated in the study and received a monetary compensation for their participation. All participants reported no neurological diseases and no history of head injury, and their visual capacity was normal or corrected to normal by MRI scanner compatible goggles. The study was approved by the ethics committee of the hospital 'Santa Maria della Misericordia' (Udine, Italy), where the MRI scans were performed. Before starting the experiment, exhaustive information about the procedure was provided and participants gave informed consent. Outside the scanner, before and after the experiment, the participants were asked for a self-reported evaluation on the dimensions of tension, sadness and anxiety, by means of a Visual Analog Scale (VAS). Specifically, the opposite ends of the three scales were respectively tagged as 'relaxed' and 'tense', 'happy' and 'sad', 'calm' and 'anxious' (in Italian, the three scales were respectively tagged as 'rilassato’ and ‘nervoso', 'felice’ and ‘triste', 'tranquillo’ and ‘ansioso'); the midpoint of each scale was also indicated. Furthermore, at the end of the experiment, general empathic tendency and alexithymic traits were measured respectively with the Interpersonal Reactivity Index (IRI) (Davis, 1980) and the Bermond-Vorst Alexithymia Questionnaire (BVAQ-B) (Vorst and Bermond, 2001). Finally, sense of presence experienced in the virtual environment was evaluated with the Igroup Presence Questionnaire (IPQ) (Schubert et al., 2001), freely available at http://www.igroup.org/pq/ipq/index.php. The IPQ is a 14-item self-report scale, subdivided in 3 subscales and a general item related to 'the sense of being there' (presence). Subscales are aimed to evaluate three independent dimensions of the VR experience, i.e. spatial presence (5 items), involvement (4 items) and experienced realism (4 items). All IPQ items are statements and respondents have to rate their degree of agreement on a 7-point Likert scale, ranging from -3 to +3.

2.2 Procedures and measures

Participants' behavior during a life-threatening situation was evaluated by using a computer-based environment developed by the Human-Computer Interaction Laboratory (HCI Lab), at the Department of Mathematics and Computer Science (University of Udine, Italy). In particular, an emergency evacuation experience of a building on fire was simulated in VR. The virtual experience was implemented using the C# programming language and NeoAxis (http://www.neoaxisgroup.com), a game engine based on the Ogre rendering engine (http://www.ogre3d.org). Participants were told to behave in the virtual environment as they would in a real-world situation and thus to evacuate the building as quickly as possible, by following the clearly visible exit signs, which reproduced accurately the familiar signs that are legally mandatory for public buildings in the participants' country (see Fig. 1C). To increase sense of presence in the simulated experience, the scenario was experienced from a first-person perspective (Slater et al., 2010; Vogeley and Fink, 2003; Vogeley et al., 2004), using fMRI-compatible goggles and earphones. Participants could move and act in the virtual environment by pressing four buttons on two fMRI-compatible response pads: index, middle and annular fingers of the right hand were used to move respectively leftward, forward and rightward, whereas index finger of the left hand was used to interact with objects in the virtual environment. Indeed, participants knew that a message appear on the lower part of the screen, whenever it was possible to perform an action on a virtual object, e.g. opening a door in front of them.

Before starting the virtual experience, participants were familiarized with buttons usage by navigating a small virtual building (Fig. 1A) and interacting with objects in it. For instance, when a participant approached a closed door, the word 'open' ('apri' in Italian) was displayed in the lower part of the screen and (s)he could decide to open the door by pressing the button on the left pad. At the end of this familiarization phase, participants were asked to lift and move away three boxes placed in an empty room of the environment. When approaching any of the three objects, the word 'push' ('spingi' in Italian) appeared on the screen (Fig. 1A). To simulate the effort needed for successfully moving the box, the participant had to repetitively press the button on the left pad, until the object moved (41 button presses were required to move away the object). The time to successfully move each of the three objects (MovingTime) was recorded to measure variability in the speed of button presses across participants. The familiarization phase ended when the participant moved all three boxes. The participant was then virtually placed in a meeting room (Fig. 1B) of a large building, together with three virtual humans; (s)he was told that the virtual humans were avatars controlled by other human participants, who were going to perform the same task from computers located in another building (Department of Mathematics and Computer Science). In fact, the movements of the virtual humans were pre-programmed and controlled by the computer application. The participant was free to explore the meeting room for about a minute and observe the behaviors of the other virtual humans (see Video1, included as Supplementary Material). If (s)he approached the virtual humans, they did not engage in social interaction but continued to move in the environment or stare at objects or from windows. The task started when a voice message on the public address system and a subsequent emergency bell alerted the participant that a fire had broken out in the building and all people had to evacuate it immediately by following the emergency signs (see Fig. 1C). Throughout the simulation, visual and auditory cues were delivered to provide aversive feedback and to increase the feeling of danger and unpleasant emotions (see Video2, included as Supplementary Material). In particular, the emergency bell and the speaker voice were repeated and the participant ran into smoke and fire along the way. Furthermore, the participant heard the sound of her/his own avatar coughing due to smoke inhalation and the visual field was reduced when (s)he was in danger, to simulate tunnel vision phenomena that occur in high stress conditions. Finally, participants were warned about the risk to their life by a bar indicating their remaining 'life energy' (see Fig. 1C). Using aversive visual and auditory feedback similar to that summarized above was found to be effective in creating an experience of risk and danger in VR (Chittaro and Zangrando, 2010).

Toward the end of the path to exit the building, participants unexpectedly encountered an injured male virtual human previously seen in the meeting room but now lying on the floor, trapped under a heavy cabinet and asking for help (see Fig. 1C). Each participant was thus faced with the dilemma of either exiting the building without stopping or spending time at the possible cost of his/her own life to help the trapped virtual human, by moving away the heavy cabinet (see Video3, included as Supplementary Material). The amount of effort to move away the cabinet and free the virtual human was set to 150 button presses. When the participant engaged in the attempt to move the cabinet, two stimuli emphasized the presence of danger: (i) a flashing red aura in the peripheral visual field, and (ii) heartbeat sound at a progressively increasing frequency, played through the headphones. Note that from the beginning of the evacuation, the energy bar decreased at the same rate for each participant, thus they all had the same very low amount of 'life energy' left when they encountered the trapped virtual human. Furthermore, if a participant stopped to rescue the virtual human, the bar kept decreasing, although the decrease was controlled in such a way that the participant could not “die” in the virtual experience.

The time taken by participants to reach the virtual human from the beginning of the evacuation (EncounterTime) was recorded and participants' behavior was evaluated by observing their actions towards the trapped virtual human. In particular, participants can be divided in three groups: (i) those who stopped and successfully helped the virtual human (SuccessfulHelp (SH) group), (ii) those who stopped and started helping, but then left before moving the cabinet away completely, without freeing the virtual human (UnSuccessfulHelp (UnSH) group), (iii) those who passed by without stopping (NoHelp (NoH) group). The emergency experience ended when participants moved away from the point of encounter with the virtual human and approached the emergency exit, with the scene fading away automatically.

At the end of the experiment, participants were informally debriefed about their experience in the virtual environment, in particular about the fact that the virtual humans were controlled by the computer application. None of them openly reported to have been suspicious about the experimental procedure.

2.3 Image acquisition and preprocessing

Blood-oxygen-level-dependent (BOLD) functional images were obtained while the task was performed. A 3-Tesla Philips Achieva whole-body MR Scanner, equipped with an 8-channel head coil, was used for MRI scanning. Structural images were acquired as 180 T1–weighted transverse images (0.75 mm slice thickness). Functional images were acquired using a T2*-weighted echo-planar imaging (EPI) sequence with 33 transverse slices covering the whole brain (slice thickness 3.2 mm; interslice gap 0.3 mm; TR/TE=2000/35ms; flip angle=90°, field of view=230x230 mm^2; matrix size=128×128, SENSE factor 2). Volume acquisition started synchronously with the beginning of the task (first emergency bell) and continued until the participant completed the evacuation. Three 'dummy' scans were acquired and discarded for the subsequent analysis. Given the self-paced duration of the virtual experience, a different number of volumes was obtained for each participant (M = 159, SD = 36). Statistical parametric mapping software (SPM8, http://www.fil.ion.ucl.ac.uk/spm/software/spm8/) was used for the pre-processing of the fMRI data. Data were corrected for head movement artifacts by rigid-body volume realignment, spatially normalized into the standard Montreal Neurological Institute (MNI) space, and spatially smoothed with 8x8x8 mm^3 full width at half-maximum (FWHM) Gaussian kernel.

2.4 Group spatial ICA for fMRI data

To avoid possible confounds due to different sample sizes, gICA as well as the statistical tests on independent components (ICs), behavioral measures and questionnaires were performed considering only the two groups with comparable numbers of participants, precisely the SH and NoH groups (see paragraph "3.1 Behavioral results").

Datasets of equal length were considered for each participant. The volume that corresponded to the encounter with the trapped virtual human was considered as volume 0. This was specifically chosen because the present study focused on brain processes related to this event. Then, considering the number of volumes acquired for the fastest participant reaching the virtual human and the fastest one completing the whole virtual experience, 111 volumes before and 5 volumes after volume 0 were selected and further analyzed (see Fig. 1C).

Group spatial ICA (Calhoun et al., 2009) was used to decompose the data into components using the Group ICA for fMRI Toolbox (GIFT - http://mialab.mrn.org/software/gift/), developed by Calhoun and colleagues (2001). According to this method, gICA was basically performed in three steps: i) dimensionality of the data was reduced for each participants and then datasets were temporally concatenated, ii) the independent sources were extracted using the Infomax algorithm (Bell and Sejnowski, 1995), iii) datasets were back-reconstructed, in order to produce subjects-specific IC maps and time courses. The dimensionality for the set of 35 fMRI acquisitions was estimated by using the minimum description length (MDL) criteria, modified to account for spatial correlation (Li et al., 2007) and then reduced by applying a 2-steps Principal Component Analysis (PCA) before temporal concatenation and gICA. At the end, 26 spatially-independent IC maps and the respective time courses were created for each participants, after gICA and back-reconstruction. Each resulting group IC map was thresholded performing a voxel-wise one-sample Student's *t*-test (Calhoun et al., 2001). Specifically, for each IC, back-reconstructed single-participant spatial maps entered the test and the resulting t-map was thresholded at $p < 0.05$, corrected for multiple comparisons according to the family-wise error approach (FWE-corrected). Finally, each of the 26 components was visually inspected and compared with components previously described in the literature (see for example Beckmann, 2012; Shirer et al., 2012; Laird et al., 2011; Calhoun et al., 2008; Cole et al., 2010; Smith et al., 2009). Nine ICs were selected as biologically meaningful, non-artifactual networks.

To better investigate differences among ICs of the SH and NoH groups, a single gICA was performed for each group separately, using the GIFT toolbox (Celone et al., 2006; Harrison et al., 2008a; Harrison et al., 2008b). This approach was meant to reduce the bias in extracting components from groups with different sample sizes (see paragraph "3.1 Behavioral results"). Furthermore, to prevent from splitting components in different sub-systems in the single-group gICA, the number of ICs to be extracted was set to be 26, equal to that of the previous analysis. Finally, the components from each groups with the highest spatial correlation (Pearson's r range = 0.40 to 0.96) to the spatial maps of the previously identified nine components were selected. In other words, the nine ICs identified using fMRI data from all the participants were used as templates for choosing and matching the components extracted performing gICA for each group separately.

Differences in IC maps between the SH and NoH groups were assessed by means of independent two-sample Student's *t*-tests. All results were thresholded at $p < 0.05$ (voxel-wise FWE-corrected).

2.5 Statistical analyses of behavioral data and questionnaires

Differences in MovingTime and EncounterTime between SH and NoH participants were analyzed with independent two-sample Student's *t*-tests. Four separate multivariate analysis of variance (MANOVA), with GROUP ('SH' and 'NoH') as between-subjects factor, were performed to analyze the IRI scores for each of the four subscales (Fantasy, Empathic Concern, Perspective Taking, and Personal Distress), the BVAQ-B scores for the five subscales (Verbalizing, Fantasizing, Identifying, Emotionalizing and Analyzing), the IPQ scores and the self-reported evaluation of tension, sadness and anxiety. In the latter case, the ratings at the beginning of the experiment ($tension_{pre}$, $sadness_{pre}$, $anxiety_{pre}$) and the difference between post- and pre-scanning ratings ($tension_{diff}$, $sadness_{diff}$ and $anxiety_{diff}$) entered the MANOVA as dependent variables.

The level of significance was set at $p < 0.05$ and all the analyses were carried out by using SPSS for Windows, version 21.0 (SSPS Inc, Chicago, Illinois, USA).

3 Results

3.1 Behavioral results

The present study aimed to investigate the prosocial or selfish moral choices made by healthy participants in a simulated life-threatening situation. According to their behavior after encountering the virtual human trapped under the cabinet, participants were subdivided in three groups: 16 out of 43 participants saved the trapped virtual human (SH group), 19 passed by without helping (NoH group), whereas the remaining 8 participants stopped to help, but then left prematurely without freeing the virtual human (UnSH group). Given that the sample sizes of the three groups were not consistent (with the SH and NoH groups of similar sizes, but substantially different from the UnSH group) and that these differences could have possibly affected the statistical power of the planned tests, data from the UnSH group were discarded and not analyzed further.

Fig. 2A shows a graphical representation of the total number of participants in each group and the number of females and males in each of them. In particular, the female to male ratios were similar in the SH group and the NoH group (respectively 11:5 and 12:7) and a chi-squared test did not show any significant differences between the two groups (Pearson's $\chi^2 = 1.21$, $p = 0.728$).

Participants in the two groups of interest showed no significant differences in interacting with objects in the virtual environment. Mean values of the variable recorded during the familiarization phase (MovingTime; Fig. 2B) were similar between the two groups (SH: $M = 11.6$, $SD = 7.7$; NoH: $M = 13.2$, $SD = 12.9$) and independent two-sample t-test showed no significant differences ($t_{33} = -0.435$, $p = 0.666$). The mean time participants spent to reach the virtual human (EncounterTime; Fig. 2C) was also similar in the two groups. Specifically, the SH group encountered the virtual human 282.7 ($SD = 42.0$) seconds after the beginning of the evacuation, and the NoH group after 284.1 ($SD = 93.1$) seconds. Independent two-sample t-test on EncounterTime showed no significant differences ($t_{33} = -0.053$, $p = 0.958$)

The statistical analyses on the self-reported questionnaires showed no significant differences between the SH and NoH groups. Bar graphs representing the mean scores for each questionnaire and the three negative emotional scales are reported in Supplementary Fig. S1, whereas numerical values and results of the multivariate tests are reported in Supplementary Tables S1-S5.

3.2 ICA results

The spatial map and the time course of each of the 26 independent components (IC) found by the group independent component analysis (gICA) were visually inspected and compared with maps and time courses of ICs already published in the literature (see for example, Calhoun et al., 2008; Cole et al., 2010). Seventeen of these components were discarded because they did not include clearly identifiable neuronal sources or they accounted for non brain-derived sources of signal, such as maps that showed head movements artifacts or ventricle regions. The remaining 9 components were investigated both for similarities and differences across the three groups of participants.

IC1 - Component 1 included the left and right primary sensorimotor areas located laterally in the precentral and post central gyri and medially in the paracentral lobule, with peaks of maxima IC weight at [-34,-30,58] and [28,-42,62] in the lateral sides and at [8,-36,64] in the medial wall (Fig. 3A). The latter comprised also the supplementary motor cortex [0,-6,56], whereas a second significant cluster was found in the cerebellum [-4,-56,-2]. The complete list of brain areas included in the IC1 is reported in Supplementary Table S6.

IC2 - The results showed a significant cluster (Fig. 3B) comprising voxels in the left inferior, middle and superior frontal gyri (respectively at [-4,8,30], [-22,10,52] and [-22,52,8]), in the left precentral gyrus ([-36,0,54]) and the supplementary motor cortex ([-2,20,56]). Furthermore, this component included also the bilateral parietal lobules (main peaks at [-36,-58,50] and [32,-50,44]). Finally, a cluster of significant voxels was also observed in the right frontal cortex, in particular in the precentral and the inferior frontal gyri (respectively at [50,6,28] and [34,6,30]). This cluster was less extended than the one in the left hemisphere; it comprised 3133 significant voxels, whereas the contralateral one included 13545 voxels. The complete list of brain areas included in the IC2 is reported in Supplementary Table S7.

IC3 - IC3 comprised a fronto-parietal network lateralized in the right hemisphere (Fig. 3C). In particular, the two main clusters included in this IC were centered in the right superior frontal gyrus and in the inferior parietal lobule, respectively at [18,30,46] and [42,-56,44]. The complete list of brain areas included in the IC3 is reported in Supplementary Table S8.

IC4 – A cluster of voxels was found to be significant in the temporal lobes (Fig. 3D). The brain structures comprised the bilateral rolandic operculum ([-60,0,10] and [62,0,12]) and the bilateral middle and superior temporal gyri (respectively at [-56,-28,4] and [66,-14,-10], and at [-60,4,-8] and [62,-16,4]). It is worth noting that this component extended in much of the superior and middle temporal lobe and its temporal dynamic was strictly related with the encounter with the trapped virtual human (see Fig. 3D). The complete list of brain areas included in the IC4 is reported in Supplementary Table S9.

IC5 and IC6 - Two independent components accounted for the functional connectivity of the BOLD signal in visual areas and the visual-processing cortical regions (Fig. 3E and Fig. 3F). The magnitude of IC5 peaked at [8,-90,4] in the right calcarine cortex (Fig. 3E), but it also comprised the left primary visual cortex (peak at [-6,-94,6]). The activity of extrastriate visual areas was segregated in a second component (IC6; Fig. 3F); in particular, significant voxels were observed bilaterally in the fusiform gyrus ([-30-62,-16] and [34,-56,-12]), and in the middle and inferior occipital gyri (respectively at [-32,-92,8] and [36,-84,6], and at [-48,-66,12] and [42,-68,10]). The complete lists of brain areas included in the IC5 and IC6 are reported in Supplementary Tables S10 and S11, respectively.

IC7 – A single independent component (Fig. 4A) included the bilateral anterior insula ([-42,10,-4] and [34,18,2]) and the anterior mid cingulate cortex ([-2,32,26] and [4,40,12]), together with subcortical structures, like the thalamus ([-6,-16,0]) and the cerebellum ([10,-60,-16]). The complete list of brain areas included in the IC7 is reported in Supplementary Table S12.

IC8 and IC9 - The neuronal sources that contributed to the default-mode network (DMN) were split in two components (Fig. 5A and Fig. 5B). On the one hand, IC8 accounted mainly for the activity in the frontal pole and comprised the bilateral superior medial frontal gyri ([-2,58,24] and [4,46,50]). Furthermore, it extended on the lateral surfaces of both hemispheres, including the superior frontal gyri ([-14,24,58] and [18,56,30]). A significant cluster was also observed caudally, in the posterior cingulate cortex/precuneus at [-2,-54,32]. Notably, the temporal dynamic of this component was strictly related with the encounter with the trapped virtual human (see Fig. 5A).

On the other hand, IC9 comprised the sources in the posterior medial surfaces of the brain. The main cluster of this IC was centered in the posterior cingulate cortex and in the precuneus, respectively [-6,-42,32] and [-6,-54,22], although other clusters of significant voxels were also observed in the lateral surfaces, specifically in the left and right angular gyri at [-44,-60,30] and [56,-60,30], and in the superior medial frontal cortex (peak at [4,62,-2]). The complete lists of brain areas included in the IC8 and IC9 are reported in Supplementary Tables S13 and S14, respectively.

3.3 Differences in network activity between groups

Differences between the two groups of participants were assessed by performing a separate independent two-sample Student's *t*-test for each component. Differences were found to be significant in 2 of the 9 ICs previously described and therefore the differences among pairs of groups were further investigated in these networks.

The network comprising the bilateral insula and the cingulate cortex (IC7; Fig. 4B) showed reduced IC weights in the SH group compared to the other group, mainly in the anterior mid cingulate cortex at [-8,36,20], but also in the anterior insula bilaterally (peaks at [-40,20,4] and [46,-4,4]). Conversely, the SH group showed higher activity in a right cluster of voxels encompassing the superior temporal, the postcentral and the supramarginal gyrus (mean peak of activation in [66,-30,28]; Fig. 4C). The complete lists of significant voxels are reported in Supplementary Table S15 for the contrast SH group < NoH group and in Supplementary Table S16 for the contrast SH group > NoH group.

Participants in the SH group also showed significant differences in IC8 when compared with the NoH group. Specifically, significant voxels were found in the medial orbito/prefrontal and anterior cingulate cortices, respectively at [4,42,-4] and [-6,40,-6], for the comparison SH group greater than the NoH group (Fig. 5C), while a lateral cortical area was identified in the opposite comparison, SH group smaller than NoH group (peak in the left middle frontal gyrus at [-40,10,58]; Fig. 5D). The complete lists of significant voxels are reported in Supplementary Table S17 for the contrast SH group > NoH group and in Supplementary Table S18 for the contrast SH group < NoH group.

4 Discussion

Studying the neural underpinnings of altruistic behavior in highly salient and ecologically valid environments is one of the major challenges of modern social cognitive neuroscience. In the present study, by combining a VR-based experimental methodology with 'model-free' analysis of fMRI data, we were able to detect patterns of functional connectivity associated with the flowing experience in a stressful situation requiring to engage in prosocial decision-making. More importantly, we were able to observe that prosocial behavior varies between participants and that this variability is predicted by differential connectivity in dedicated functional brain networks.

The overall VR experience was associated to functional brain networks previously identified in the literature during both resting state and active tasks (Calhoun et al., 2008; Bressler and Menon, 2010; Arbabshirani et al., 2012), as revealed by gICA. In particular, networks related to the processing of the basic features of sensory stimuli (visual and auditory) and to higher-order cognitive functions, such as the planning and execution of actions were detected. Indeed, on one hand, clusters of functional connected regions were found both in primary and secondary sensory areas, and in motor areas, whereas on the other hand, higher-order cognitive networks were also detected, such as the attentive fronto-parietal and the default-mode networks (Laird et al., 2011; Smith et al., 2009).

Interestingly, only two of the identified networks showed significant differences between the participants who succeeded in acting prosocially and those who did not. Specifically, differences in functional connectivity were observed in the network including the anterior insula (AI) and anterior mid cingulate cortex (aMCC), with weaker connectivity of these areas in the group of participants who acted prosocially compared to those that failed, and increased activity in a cortical domain at the border between superior temporal and supramarginal gyri, in the right hemisphere. Furthermore, the prosocial group showed greater activity in a second functional network including the medial orbito/prefrontal and the anterior cingulate cortices.

It has been suggested that an automatic emotional response, evoked by the observation of another individual's suffering, could drive the decision of helping the person in need and therefore acting prosocially. In other words, empathic processes motivate the costly aiding behavior and the empathy-altruism hypothesis was proposed as a reference framework to study this distinguishing human behavior (Batson et al., 1991; Hein et al., 2010; Singer and Lamm, 2009). Hein and colleagues (2011), for example, reported that the autonomic emotional response (evaluated by skin conductance) in participants who witnessed other participants suffering predicted their willingness to share the other's pain. The empathy-altruism hypothesis has led neuroscientists to investigate the role of empathy-related cortical regions, such as AI and aMCC, in prosocial behavior and the possibility that the activity in these brain structures might predict the tendency to act with the intention to help others (Lamm and Singer, 2010). Although several findings have linked altruism with the brain network underlying our capacity to understand and share others' emotional states (Masten et al., 2011; Rameson et al., 2012; Hein et al., 2010; Morishima et al., 2012; Waytz et al., 2012), some authors have pinpointed the role of factors other than empathic processes as motivators of prosocial behavior (Fahrenfort et al., 2012). This stems from the findings that in some cases the link between empathy and prosocial behaviors was inconsistent. Singer and collaborators (2008), for example, failed to show an association between activity of empathic-relevant regions and prosocial tendencies. In that study, the volunteers interacted in an economic game and subsequently were subdivided in two groups (prosocial and selfish) according to their tendency to cooperate. The authors found that the prosocial group did not show higher BOLD signal in AI or aMCC compared to the selfish group when witnessing another person suffering. Interestingly, as the authors pointed out, other causes like the willingness to avoid negative social consequences may motivate the desire to increase the wellbeing of others and therefore may explain the lack of a relation between empathic brain responses and altruistic tendencies. In other words, factors that may prompt to avoid helping should be also considered, in addition to processes that lead toward prosocial behaviors. In this sense, contextual factors and self-referenced emotional state could be relevant for determining the other-oriented choices. For example, the situation in which a person is seeking for help could be perceived as a threat to the self and the high personal distress may evoke an egoistic motivation that leads to reduce one's own aversive arousal by escaping without helping (Batson et al., 1987). Therefore, two opposite processes could operate in social decision-making (Paciello et al., 2013): one might be initiated by empathic response and lead to altruistic decisions, the other might be related to the evaluation of the situation as excessively costly and stressful, thus resulting in selfish behaviors.

The results of our study can be discussed in the light of this hypothesis. In particular, the simulated dangerous situation was possibly perceived as a stressful event for the participant, resulting in the decision not to risk personal damage and therefore act selfishly. The higher degree of functional connectivity within and between AI and aMCC in the group that did not help the virtual human in comparison to the group that did could therefore reflect the higher level of personal distress in those participants who decided to escape. Note that the temporal dynamic of this network was not strictly related to the encounter with the trapped virtual human, but instead showed a constant activity throughout the entire virtual experience. This further suggests that the activity in the AI and aMCC during the task execution reflected the processing of the high level of risk and threat to the self, leading to a self-centered behavioral response. This hypothesis is supported by evidence showing that AI is involved in monitoring the risk and evaluating the error in risk prediction (Preuschoff et al., 2008; Singer et al., 2009) and that the cingulate cortex is involved in autonomic arousal responses that accompany and perhaps guide cognition and behavior (Critchley, 2004). The activity of AI and aMCC has been associated not only to the representation of internal bodily states and interoception (Craig, 2003), but also to the processing of the salience inherently embedded in any internal and external stimulus (Mouraux et al., 2011; Laird et al., 2011; Legrain et al., 2011). Indeed, the intrinsic connectivity network comprising these two cortical areas has been referred to as 'salience network' (Seeley et al., 2007). The functional connectivity within the salience network has been shown to correlate with anxiety state, rated by participants who were about to begin a task-free fMRI scan (Seeley et al., 2007). Interestingly, in our study the participants who behaved prosocially were those who reported the higher (although not statistically significant) reduction in the anxiety level at the end of the experiment (see Supplementary Fig. 1A). It has also been demonstrated that this network acts as a top-down control system whose activity is relatively stable across tasks and therefore it is supposed to provide a 'set-maintenance' and monitoring signal (Dosenbach et al., 2008). Finally, Markett and colleagues (2013) found a positive correlation between the activity of the network encompassing the AI and aMCC and self-reported scores of harm avoidance, suggesting a relationship between the functional connectivity in this network and a trait of personality (namely the anxiety trait).

The second network found to be functionally different between the two groups of interest, with greater degree of connectivity in the prosocial group, included the medial orbitofrontal and anterior cingulate cortices. In the neuroscience literature, activity in the mPFC has been associated with the human ability of taking the perspective of other individuals (Jackson et al., 2006; Decety and Sommerville, 2003) and inferring their mental state (Bzdok et al., 2013; Mitchell et al., 2005). Moreover, neuroimaging and brain lesion studies have linked these structures (in particular the orbitofrontal portion) with moral cognition and moral decision-making (Koenigs et al., 2007; Anderson et al., 1999; Greene et al., 2001). To behave prosocially, the other individual has to be recognized as an entity capable of conscious experience, action and with specific mental and emotional states. Therefore, it has been hypothesized that the human ability of inferring mental disposition is fundamental for altruistic behavior. According with this hypothesis, several studies have demonstrated the involvement of the medial prefrontal cortex in altruistic decision (Waytz et al., 2012), with a positive correlation between the activity in this area and the preference of prosocial choices (Mathur et al., 2010; Moll et al., 2006; Rilling et al., 2002).

Our results support the hypothesis that a greater activity in mPFC leads to behave prosocially. Interestingly, the temporal dynamic of this network was strictly related with the encounter with the trapped virtual human, unlike what was observed for the salience network. Therefore, the mPFC seems to underlie cognitive functions that are initiated by an external socially-relevant stimulus, such as taking the perspective of the other person or the evaluation of the different moral choices.

A second hypothesis may be put forward to explain the significant findings in the mPFC. Indeed, the way participants behaved in VR could have been affected by concerns about good reputation (and not concerns about the welfare of the virtual human) and they could have behaved altruistically in order to increase it. Consequently, it is possible that the social information elaborated by the mPFC in this case might be that needed for a third-person perspective taking and for elaborating how the experimenter would judge the participant on the basis of her or his decision regarding the virtual human. Evidence supporting this role of the mPFC has demonstrated that this region, in particular its most anterior part, is active when a person has to think how oneself is represented by another one (Amodio and Frith, 2006; Frith and Singer, 2008; Izuma et al., 2010). Although our data do not allow us to definitely endorse one hypothesis over the other, they still support the idea that mPFC has a pivotal role in social cognition and in processing information relevant for social goals and behaviors which can affect other individuals (Denny et al., 2012; Amodio and Frith, 2006; Bzdok et al., 2013).

Together, the results observed in the mPFC and in the salient network lead to speculate an interplay between these two networks in the context of our experiment and that their interaction is likely to determine the behavioral response of participants in the threatening situation simulated during the virtual experience. The activity of mPFC prompts to helping behavior; conversely, the AI and aMCC seem to be responsible for the evaluation of risk during the entire task and the prevailing self-oriented choice.

It is worth noting that another network showed an activity timecourse that peaked after the encounter with the virtual human. This network comprised the superior temporal gyrus (STG) bilaterally. Investigations in animals and humans have related the role of the superior temporal cortex to social perception, in particular the processing of those sensory stimuli components that are important for social interaction or analysis of the intentions of other individuals (Allison et al., 2000; Hein and Knight, 2008; Strobel et al., 2008). Indeed, the observation of significant activity in STG (similarly engaged by all the participants) in concomitance with the encounter with the trapped virtual human suggests that the event was a highly relevant and novel social stimulus, whose processing would end with the participant's decision of risking or not his/her own life in the virtual experience to save the virtual human.

Finally, the temporoparietal junction (TPJ) was observed to be statistically more active in the prosocial group than in the other group. This area has been shown to be involved in social cognitive processes, such as mentalizing, self/other distinction, and more generally other-oriented behavior (Jackson et al., 2006; Decety and Sommerville, 2003; Decety and Lamm, 2007). Recently, Morishima and colleagues (2012) have demonstrated a close relationship between the right TPJ and the tendency to behave altruistically. In our study, the observation of the different engagement of this area between groups suggests its role in a general predisposition to act altruistically and thus facilitating the decision to help the trapped virtual human.

Although we cannot draw definitive conclusions about the involvement of brain networks such as the salience network and mPFC in driving prosocial behaviors, we provided a first example of how a more ecologic setting can be implemented to investigate complex social decision-making in humans. Notably, our study might inspire new hypotheses or experimental protocols based on different neurophysiological techniques, which will substantially help to disentangle the causal relations between the social context here investigated and the underlying neurobiological substrates. For instance, modified versions of our VR paradigm could be implemented to investigate how prosocial attitudes depend on specific features of both the agent and the person in need (i.e., age, gender, etc.). Some insights about the effect of gender in the present experimental context could be drawn from the observation that participants of both genders engaged in similar helping behaviors, although the current study was not aimed to address this issue systematically. In the past, several studies have focused on the role played by gender, age or group membership on the tendency to behave prosocially (Eagly, 2009; Eagly and Becker, 2005; Eisenberg and Miller, 1987; Eisenberg and Lennon, 1983; Mathur et al., 2010; Hein et al., 2010) suggesting that gender and age have an effect on mental processes that are crucial for eliciting helping behaviors, such as the empathic response or the capacity to detect pain-related cues in facial expressions (Groen et al., 2013; Michalska et al., 2013; Eisenberg and Lennon, 1983; Riva et al., 2011; Coll et al., 2012). Although these studies have provided insights about prosocial behaviors, new paradigms like the one presented in the current study will allow researchers to better clarify the complex mental processes and the neurobiological basis underlying prosocial decisions.

5 Limitations

Although our study stands for its novelty in applying the ICA approach on fMRI data acquired in a virtual environment, particularly in the field of social neuroscience, it has some limitations that should be kept in mind when discussing its neurophysiological findings.

Firstly, it should be considered that ICA does not allow one to easily draw inference at a group level (Calhoun et al., 2009) and different approaches have been proposed to tackle the issue, each one with its own advantages and drawbacks (Calhoun et al., 2009; Cole et al., 2010). Secondly, a common issue these methods try to deal with is how to separate biological meaningful components from those that account for artifacts (i.e., head movements, high-frequency noise). In the present study, only 9 out of 26 components were selected and considered in the statistical analysis. Although the final number of selected ICs was comparable with that of previously published studies investigating functional networks either at rest or during tasks (Harrison et al., 2008b; Cole et al., 2010; Chen et al., 2008; Laird et al., 2011; Shirer et al., 2012), it might be possible that our approach was too conservative and thus some neuronal-related components were missed.

Finally, an issue related to our VR-based paradigm is to what extent the participants perceived the virtual environment as a real-world situation or as an artificial videogame-like experience. Although we sought to create a vivid VR setting close to a real experience (as indicated by positive ratings for both the "spatial presence" and the "general sense of presence" subscales; see Supplementary Fig. S1) and all participants were expressly instructed to behave as naturally as possible, it should be noticed that they also reported low mean ratings for the IPQ "Experienced realism" subscale (see Supplementary Fig. S1C). This may raise some questions about what mental processes are responsible for prosocial behavior when the participants encountered the trapped virtual human. For example, participants' behavior could be driven by reputation concerns as well as by a real understanding of the affective and mental state of an individual in danger.

6 Conclusion

The aim of the present study was to investigate the neurophysiological underpinnings of altruistic behaviour in a more ecological context. The highly realistic scenario created with virtual reality, combined with the Independent Component Analysis of fMRI data, allowed us to observe online brain activity during a flowing stressful experience that required social decision making. For the first time, we were able to disentangle the interplay of dedicated brain networks in the engagement (or not) of prosocial behaviour, bringing new evidence of the mechanisms of altruistic behaviour in a close-to-real-life situation.

7 Acknowledgments

The authors want to thank the two anonymous reviewers for their helpful comments, which allowed us to greatly improve the quality of the manuscript.

8 Conflict of interest

The authors declare no conflict of interest.

9 References

Allison, T., Puce, A., McCarthy, G., 2000. Social perception from visual cues: role of the STS region. Trends Cogn Sci 4, 267-278.

Amodio, D.M., Frith, C.D., 2006. Meeting of minds: the medial frontal cortex and social cognition. Nat Rev Neurosci 7, 268-277.

Anderson, S.W., Bechara, A., Damasio, H., Tranel, D., Damasio, A.R., 1999. Impairment of social and moral behavior related to early damage in human prefrontal cortex. Nat Neurosci 2, 1032-1037.

Arbabshirani, M.R., Havlicek, M., Kiehl, K.A., Pearlson, G.D., Calhoun, V.D., 2012. Functional network connectivity during rest and task conditions: A comparative study. Hum Brain Mapp.

Batson, C.D., Batson, J.G., Slingsby, J.K., Harrell, K.L., Peekna, H.M., Todd, R.M., 1991. Empathic joy and the empathy-altruism hypothesis. J Pers Soc Psychol 61, 413-426.

Batson, C.D., Fultz, J., Schoenrade, P.A., 1987. Distress and empathy: two qualitatively distinct vicarious emotions with different motivational consequences. J Pers 55, 19-39.

Beckmann, C.F., 2012. Modelling with independent components. NeuroImage 62, 891-901.

Bell, A.J., Sejnowski, T.J., 1995. An information-maximization approach to blind separation and blind deconvolution. Neural Comput 7, 1129-1159.

Bernhardt, B.C., Singer, T., 2012. The neural basis of empathy. Annu Rev Neurosci 35, 1-23.

Bohil, C.J., Alicea, B., Biocca, F.A., 2011. Virtual reality in neuroscience research and therapy. Nat Rev Neurosci 12, 752-762.

Bowles, S., 2006. Group competition, reproductive leveling, and the evolution of human altruism. Science 314, 1569-1572.

Boyd, R., 2006. Evolution. The puzzle of human sociality. Science 314, 1555-1556.

Bressler, S.L., Menon, V., 2010. Large-scale brain networks in cognition: emerging methods and principles. Trends Cogn Sci 14, 277-290.

Byrne, R.W., Bates, L.A., 2007. Sociality, evolution and cognition. Curr Biol 17, R714-723.

Bzdok, D., Langner, R., Schilbach, L., Engemann, D.A., Laird, A.R., Fox, P.T., Eickhoff, S.B., 2013. Segregation of the human medial prefrontal cortex in social cognition. Front Hum Neurosci 7, 232.

Calhoun, V.D., Adali, T., Pearlson, G.D., Pekar, J.J., 2001. A method for making group inferences from functional MRI data using independent component analysis. Hum Brain Mapp 14, 140-151.

Calhoun, V.D., Kiehl, K.A., Pearlson, G.D., 2008. Modulation of temporally coherent brain networks estimated using ICA at rest and during cognitive tasks. Hum Brain Mapp 29, 828-838.

Calhoun, V.D., Liu, J., Adali, T., 2009. A review of group ICA for fMRI data and ICA for joint inference of imaging, genetic, and ERP data. NeuroImage 45, S163-172.

Celone, K.A., Calhoun, V.D., Dickerson, B.C., Atri, A., Chua, E.F., Miller, S.L., DePeau, K., Rentz, D.M., Selkoe, D.J., Blacker, D., Albert, M.S., Sperling, R.A., 2006. Alterations in memory networks in mild cognitive impairment and Alzheimer's disease: an independent component analysis. J Neurosci 26, 10222-10231.

Chen, S., Ross, T.J., Zhan, W., Myers, C.S., Chuang, K.S., Heishman, S.J., Stein, E.A., Yang, Y., 2008. Group independent component analysis reveals consistent resting-state networks across multiple sessions. Brain Res 1239, 141-151.

Chittaro, L., Zangrando, N., 2010. The persuasive power of virtual reality: effects of simulated human distress on attitudes towards fire safety. In: Ploug, T., Hasle, P., Oinas-Kukkonen, H. (Eds.), Persuasive Technology. Lecture Notes in Computer Science. Springer, Heidelberg, pp. 58-69.

Cole, D.M., Smith, S.M., Beckmann, C.F., 2010. Advances and pitfalls in the analysis and interpretation of resting-state FMRI data. Front Syst Neurosci 4, 1-15.

Coll, M.P., Budell, L., Rainville, P., Decety, J., Jackson, P.L., 2012. The role of gender in the interaction between self-pain and the perception of pain in others. J Pain 13, 695-703.

Craig, A.D., 2003. Interoception: the sense of the physiological condition of the body. Curr Opin Neurobiol 13, 500-505.
Critchley, H.D., 2004. The human cortex responds to an interoceptive challenge. Proc Natl Acad Sci U S A 101, 6333-6334.
Damoiseaux, J.S., Rombouts, S.A., Barkhof, F., Scheltens, P., Stam, C.J., Smith, S.M., Beckmann, C.F., 2006. Consistent resting-state networks across healthy subjects. Proc Natl Acad Sci U S A 103, 13848-13853.
Davis, M., 1980. A multidimensional approach to individual differences in empathy. JSAS Catalog of Selected Documents 10, 85.
Decety, J., Lamm, C., 2007. The role of the right temporoparietal junction in social interaction: how low-level computational processes contribute to meta-cognition. Neuroscientist 13, 580-593.
Decety, J., Sommerville, J.A., 2003. Shared representations between self and other: a social cognitive neuroscience view. Trends Cogn Sci 7, 527-533.
Denny, B.T., Kober, H., Wager, T.D., Ochsner, K.N., 2012. A meta-analysis of functional neuroimaging studies of self- and other judgments reveals a spatial gradient for mentalizing in medial prefrontal cortex. J Cogn Neurosci 24, 1742-1752.
Dosenbach, N.U., Fair, D.A., Cohen, A.L., Schlaggar, B.L., Petersen, S.E., 2008. A dual-networks architecture of top-down control. Trends Cogn Sci 12, 99-105.
Dunbar, R.I., Shultz, S., 2007. Evolution in the social brain. Science 317, 1344-1347.
Eagly, A.H., 2009. The his and hers of prosocial behavior: an examination of the social psychology of gender. Am Psychol 64, 644-658.
Eagly, A.H., Becker, S.W., 2005. Comparing the heroism of women and men. Am Psychol 60, 343-344.
Eisenberg, N., Lennon, R., 1983. Sex differences in empathy and related capacities. Psychol Bull 94, 100-131.
Eisenberg, N., Miller, P.A., 1987. The relation of empathy to prosocial and related behaviors. Psychol Bull 101, 91-119.
Fahrenfort, J.J., van Winden, F., Pelloux, B., Stallen, M., Ridderinkhof, K.R., 2012. Neural correlates of dynamically evolving interpersonal ties predict prosocial behavior. Front Neurosci 6, 28.
Fehr, E., Fischbacher, U., 2003. The nature of human altruism. Nature 425, 785-791.
FeldmanHall, O., Dalgleish, T., Thompson, R., Evans, D., Schweizer, S., Mobbs, D., 2012a. Differential neural circuitry and self-interest in real vs hypothetical moral decisions. Soc Cogn Affect Neurosci 7, 743-751.
FeldmanHall, O., Mobbs, D., Evans, D., Hiscox, L., Navrady, L., Dalgleish, T., 2012b. What we say and what we do: the relationship between real and hypothetical moral choices. Cognition 123, 434-441.
Frith, C.D., Singer, T., 2008. The role of social cognition in decision making. Philos Trans R Soc Lond B Biol Sci 363, 3875-3886.
Greene, J.D., Sommerville, R.B., Nystrom, L.E., Darley, J.M., Cohen, J.D., 2001. An fMRI investigation of emotional engagement in moral judgment. Science 293, 2105-2108.
Groen, Y., Wijers, A.A., Tucha, O., Althaus, M., 2013. Are there sex differences in ERPs related to processing empathy-evoking pictures? Neuropsychologia 51, 142-155.
Guye, M., Bartolomei, F., Ranjeva, J.P., 2008. Imaging structural and functional connectivity: towards a unified definition of human brain organization? Curr Opin Neurol 21, 393-403.
Harrison, B.J., Pujol, J., Lopez-Sola, M., Hernandez-Ribas, R., Deus, J., Ortiz, H., Soriano-Mas, C., Yucel, M., Pantelis, C., Cardoner, N., 2008a. Consistency and functional specialization in the default mode brain network. Proc Natl Acad Sci U S A 105, 9781-9786.
Harrison, B.J., Pujol, J., Ortiz, H., Fornito, A., Pantelis, C., Yucel, M., 2008b. Modulation of brain resting-state networks by sad mood induction. PLoS One 3, e1794.

Hein, G., Knight, R.T., 2008. Superior temporal sulcus--It's my area: or is it? J Cogn Neurosci 20, 2125-2136.
Hein, G., Lamm, C., Brodbeck, C., Singer, T., 2011. Skin conductance response to the pain of others predicts later costly helping. PLoS One 6, e22759.
Hein, G., Silani, G., Preuschoff, K., Batson, C.D., Singer, T., 2010. Neural responses to ingroup and outgroup members' suffering predict individual differences in costly helping. Neuron 68, 149-160.
Hoffman, H.G., Richards, T., Coda, B., Richards, A., Sharar, S.R., 2003. The illusion of presence in immersive virtual reality during an fMRI brain scan. Cyberpsychol Behav 6, 127-131.
Izuma, K., Saito, D.N., Sadato, N., 2010. The roles of the medial prefrontal cortex and striatum in reputation processing. Soc Neurosci 5, 133-147.
Jackson, P.L., Brunet, E., Meltzoff, A.N., Decety, J., 2006. Empathy examined through the neural mechanisms involved in imagining how I feel versus how you feel pain. Neuropsychologia 44, 752-761.
Koenigs, M., Young, L., Adolphs, R., Tranel, D., Cushman, F., Hauser, M., Damasio, A., 2007. Damage to the prefrontal cortex increases utilitarian moral judgements. Nature 446, 908-911.
Laird, A.R., Fox, P.M., Eickhoff, S.B., Turner, J.A., Ray, K.L., McKay, D.R., Glahn, D.C., Beckmann, C.F., Smith, S.M., Fox, P.T., 2011. Behavioral interpretations of intrinsic connectivity networks. J Cogn Neurosci 23, 4022-4037.
Lamm, C., Singer, T., 2010. The role of anterior insular cortex in social emotions. Brain Struct Funct 214, 579-591.
Legrain, V., Iannetti, G.D., Plaghki, L., Mouraux, A., 2011. The pain matrix reloaded: a salience detection system for the body. Prog Neurobiol 93, 111-124.
Li, Y.O., Adali, T., Calhoun, V.D., 2007. Estimating the number of independent components for functional magnetic resonance imaging data. Hum Brain Mapp 28, 1251-1266.
Lieberman, M.D., 2012. A geographical history of social cognitive neuroscience. NeuroImage 61, 432-436.
Markett, S., Weber, B., Voigt, G., Montag, C., Felten, A., Elger, C., Reuter, M., 2013. Intrinsic connectivity networks and personality: The temperament dimension harm avoidance moderates functional connectivity in the resting brain. Neuroscience 240, 98-105.
Masten, C.L., Morelli, S.A., Eisenberger, N.I., 2011. An fMRI investigation of empathy for 'social pain' and subsequent prosocial behavior. NeuroImage 55, 381-388.
Mathur, V.A., Harada, T., Lipke, T., Chiao, J.Y., 2010. Neural basis of extraordinary empathy and altruistic motivation. NeuroImage 51, 1468-1475.
McKeown, M.J., Makeig, S., Brown, G.G., Jung, T.P., Kindermann, S.S., Bell, A.J., Sejnowski, T.J., 1998. Analysis of fMRI data by blind separation into independent spatial components. Hum Brain Mapp 6, 160-188.
Michalska, K.J., Kinzler, K.D., Decety, J., 2013. Age-related sex differences in explicit measures of empathy do not predict brain responses across childhood and adolescence. Dev Cogn Neurosci 3, 22-32.
Mitchell, J.P., Banaji, M.R., Macrae, C.N., 2005. The link between social cognition and self-referential thought in the medial prefrontal cortex. J Cogn Neurosci 17, 1306-1315.
Moll, J., Krueger, F., Zahn, R., Pardini, M., de Oliveira-Souza, R., Grafman, J., 2006. Human fronto-mesolimbic networks guide decisions about charitable donation. Proc Natl Acad Sci U S A 103, 15623-15628.
Morishima, Y., Schunk, D., Bruhin, A., Ruff, C.C., Fehr, E., 2012. Linking brain structure and activation in temporoparietal junction to explain the neurobiology of human altruism. Neuron 75, 73-79.
Mouraux, A., Diukova, A., Lee, M.C., Wise, R.G., Iannetti, G.D., 2011. A multisensory investigation of the functional significance of the "pain matrix". NeuroImage 54, 2237-2249.

Paciello, M., Fida, R., Cerniglia, L., Tramontano, C., Cole, E., 2013. High cost helping scenario: The role of empathy, prosocial reasoning and moral disengagement on helping behavior. Personality and Individual Differences 55, 3-7.
Preuschoff, K., Quartz, S.R., Bossaerts, P., 2008. Human insula activation reflects risk prediction errors as well as risk. J Neurosci 28, 2745-2752.
Rameson, L.T., Morelli, S.A., Lieberman, M.D., 2012. The neural correlates of empathy: experience, automaticity, and prosocial behavior. J Cogn Neurosci 24, 235-245.
Rilling, J., Gutman, D., Zeh, T., Pagnoni, G., Berns, G., Kilts, C., 2002. A neural basis for social cooperation. Neuron 35, 395-405.
Riva, P., Sacchi, S., Montali, L., Frigerio, A., 2011. Gender effects in pain detection: speed and accuracy in decoding female and male pain expressions. Eur J Pain 15, 985 e981-985 e911.
Sanchez-Vives, M.V., Slater, M., 2005. From presence to consciousness through virtual reality. Nat Rev Neurosci 6, 332-339.
Schubert, T., Friedmann, F., Regenbrecht, H., 2001. The experience of presence: Factor analytic insights. Presence: Teleoperators and virtual environments 10, 266-281.
Seeley, W.W., Menon, V., Schatzberg, A.F., Keller, J., Glover, G.H., Kenna, H., Reiss, A.L., Greicius, M.D., 2007. Dissociable intrinsic connectivity networks for salience processing and executive control. J Neurosci 27, 2349-2356.
Shirer, W.R., Ryali, S., Rykhlevskaia, E., Menon, V., Greicius, M.D., 2012. Decoding subject-driven cognitive states with whole-brain connectivity patterns. Cereb Cortex 22, 158-165.
Silk, J.B., 2007. Social components of fitness in primate groups. Science 317, 1347-1351.
Singer, T., 2012. The past, present and future of social neuroscience: a European perspective. NeuroImage 61, 437-449.
Singer, T., Critchley, H.D., Preuschoff, K., 2009. A common role of insula in feelings, empathy and uncertainty. Trends Cogn Sci 13, 334-340.
Singer, T., Lamm, C., 2009. The social neuroscience of empathy. Ann N Y Acad Sci 1156, 81-96.
Singer, T., Snozzi, R., Bird, G., Petrovic, P., Silani, G., Heinrichs, M., Dolan, R.J., 2008. Effects of oxytocin and prosocial behavior on brain responses to direct and vicariously experienced pain. Emotion 8, 781-791.
Slater, M., Spanlang, B., Sanchez-Vives, M.V., Blanke, O., 2010. First person experience of body transfer in virtual reality. PLoS One 5, e10564.
Smith, S.M., Fox, P.T., Miller, K.L., Glahn, D.C., Fox, P.M., Mackay, C.E., Filippini, N., Watkins, K.E., Toro, R., Laird, A.R., Beckmann, C.F., 2009. Correspondence of the brain's functional architecture during activation and rest. Proc Natl Acad Sci U S A 106, 13040-13045.
Spiers, H.J., Maguire, E.A., 2007. Decoding human brain activity during real-world experiences. Trends Cogn Sci 11, 356-365.
Strobel, A., Debener, S., Sorger, B., Peters, J.C., Kranczioch, C., Hoechstetter, K., Engel, A.K., Brocke, B., Goebel, R., 2008. Novelty and target processing during an auditory novelty oddball: a simultaneous event-related potential and functional magnetic resonance imaging study. NeuroImage 40, 869-883.
Uddin, L.Q., Kelly, A.M., Biswal, B.B., Castellanos, F.X., Milham, M.P., 2009. Functional connectivity of default mode network components: correlation, anticorrelation, and causality. Hum Brain Mapp 30, 625-637.
Vogeley, K., Fink, G.R., 2003. Neural correlates of the first-person-perspective. Trends Cogn Sci 7, 38-42.
Vogeley, K., May, M., Ritzl, A., Falkai, P., Zilles, K., Fink, G.R., 2004. Neural correlates of first-person perspective as one constituent of human self-consciousness. J Cogn Neurosci 16, 817-827.
Vorst, H., Bermond, B., 2001. Validity and reliability of the Bermond–Vorst Alexithymia Questionnaire. Personality and Individual Differences 30, 413-434.

Waytz, A., Zaki, J., Mitchell, J.P., 2012. Response of dorsomedial prefrontal cortex predicts altruistic behavior. J Neurosci 32, 7646-7650.

Figures

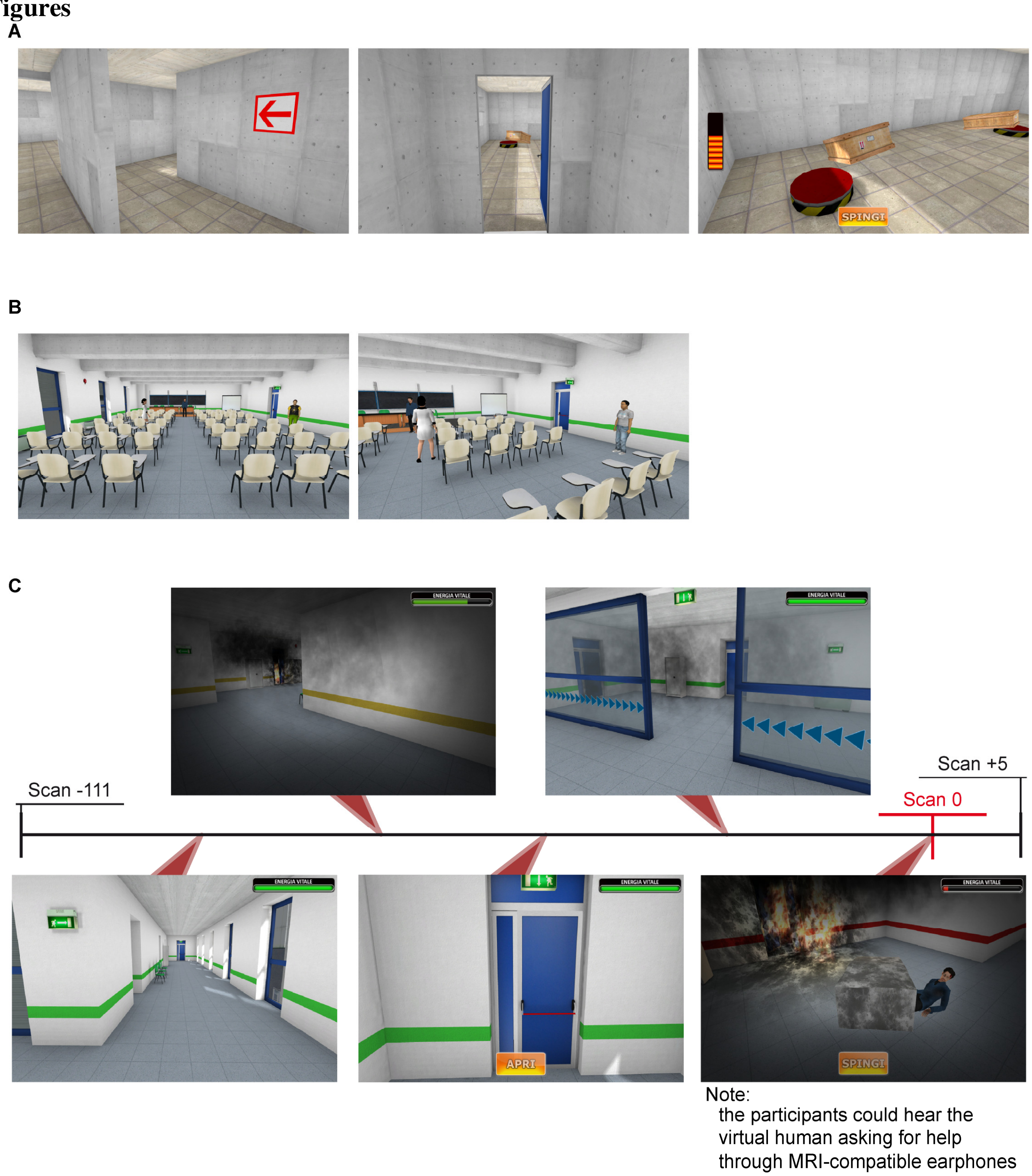

Fig. 1 - The virtual experience. (**A**) Screenshots of the initial familiarization phase session in which participants learn how to move, open doors (middle picture) and lift objects (right picture). (**B**) Screenshots of the meeting room populated by other virtual humans (the participants were told that these virtual humans were controlled by volunteers participating to the same experiment). (**C**) Representative screenshots and timeline of the task. The danger of the situation was emphasized by visual cues, such as smoke in the corridors, reduced visibility and sounds such as coughs. The encounter with the virtual human trapped by the heavy cabinet is shown in the bottom right of the picture. In each screenshot, the 'life energy' bar, which informs participants about the amount of life left, is visible in the upper right corner of the screenshot itself. The black horizontal line depicts the fMRI scans considered for the gICA (volume 0: encounter with the virtual human; volume -111: number of scans for the fastest participant in reaching the virtual human; volume +5: number of scans for the fastest participant in completing the task).

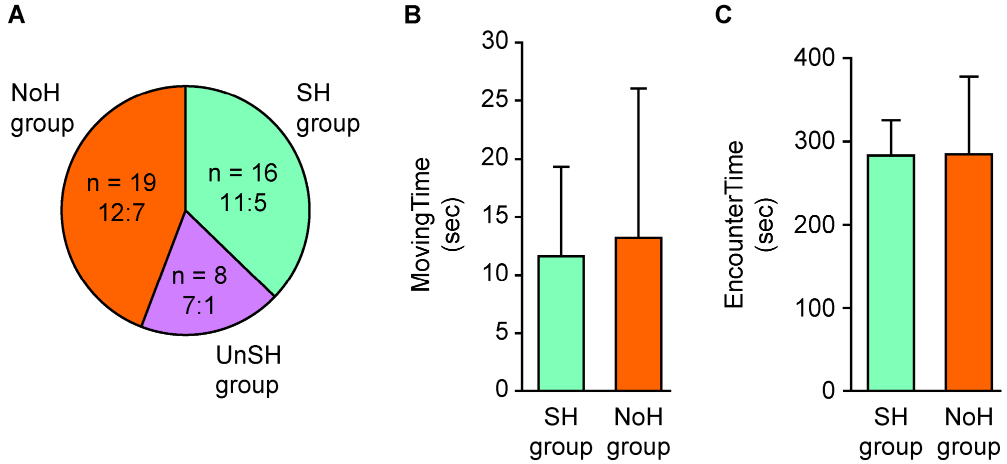

Fig. 2 – Behavioral data. (**A**) Distribution of the behavioral responses in the overall group. According to their behavior, participants were classified in NoH group, those who passed by the virtual human without helping; SH group, those who stopped and successfully helped the trapped virtual human; and UnSH group, those who started helping, but abandoned the virtual human before freeing it. The ratio indicates female to male participants. (**B**) Means and standard deviations of the MovingTime variable for the two groups with similar sample size. (**C**) Means and standard deviations of the EncounterTime variable for the two groups with similar sample size.

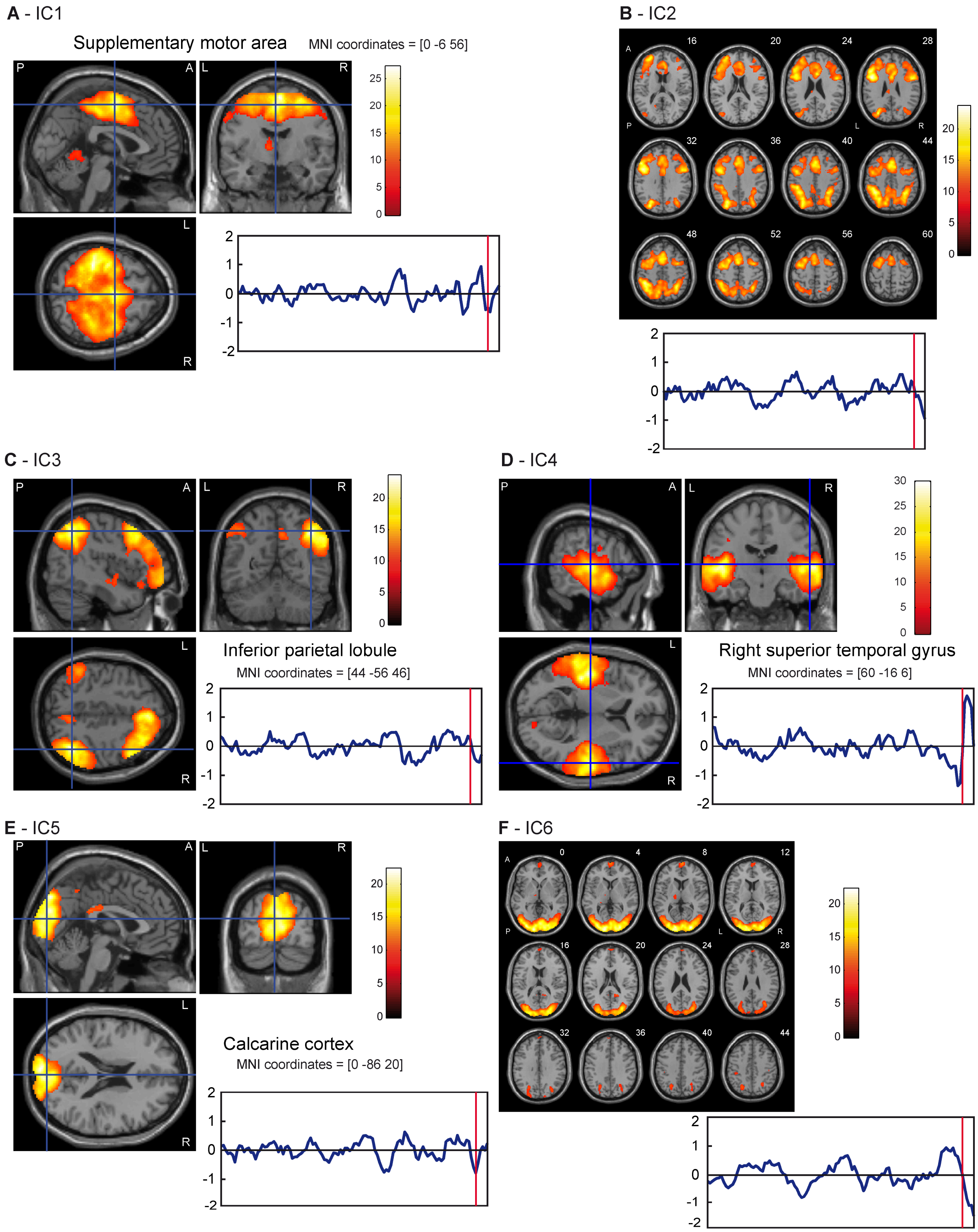

Fig. 3 – Functional connectivity data. The functionally relevant independent components (ICs) resulting from the gICA conducted on the datasets of the two groups are shown; these independent components did not show significant group differences. According to the existing literature, they were labeled as: (**A**) the somatosensory network, (**B**) the visuospatial network, (**C**) the right executive control network, (**D**) the auditory network, and two networks comprising respectively (**E**) the primary visual areas and (**F**) the higher-order extrastriate visual areas. Thresholded statistical maps and time courses are depicted for each IC. Statistical maps were thresholded at $p < 0.05$, corrected for family-wise error; the color bars represent *t* values. MNI coordinates (in mm) refer to the crosshair. A = anterior; L = left; P = posterior; R = right.

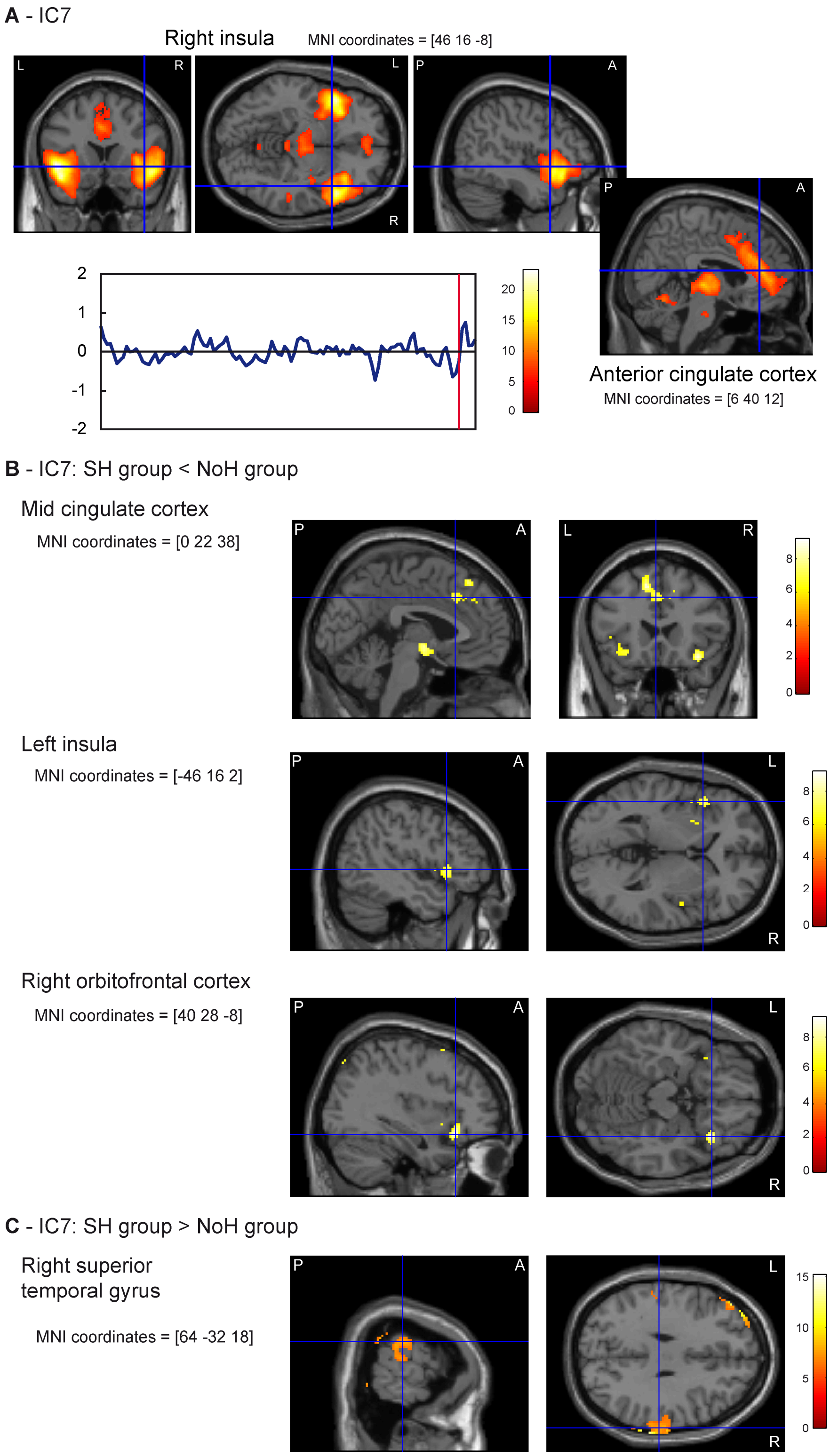

Fig. 4 - Salience network. (**A**) the spatial map and time course of the independent component commonly observed in the three groups that includes the insula and the cingulate cortex. Some nodes of this network show significant differences between the participants who saved the virtual human (SH group) and those who did not (NoH group). Specifically, functional connectivity in the first group was decreased in the cingulate cortex, the left insula and the right orbitofrontal cortex (**B**), whereas increased in the right superior temporal gyrus (**C**). Statistical maps were thresholded at $p < 0.05$, corrected for family-wise error; the color bars represent t values. MNI coordinates (in mm) refer to the crosshair. A = anterior; L = left; P = posterior; R = right.

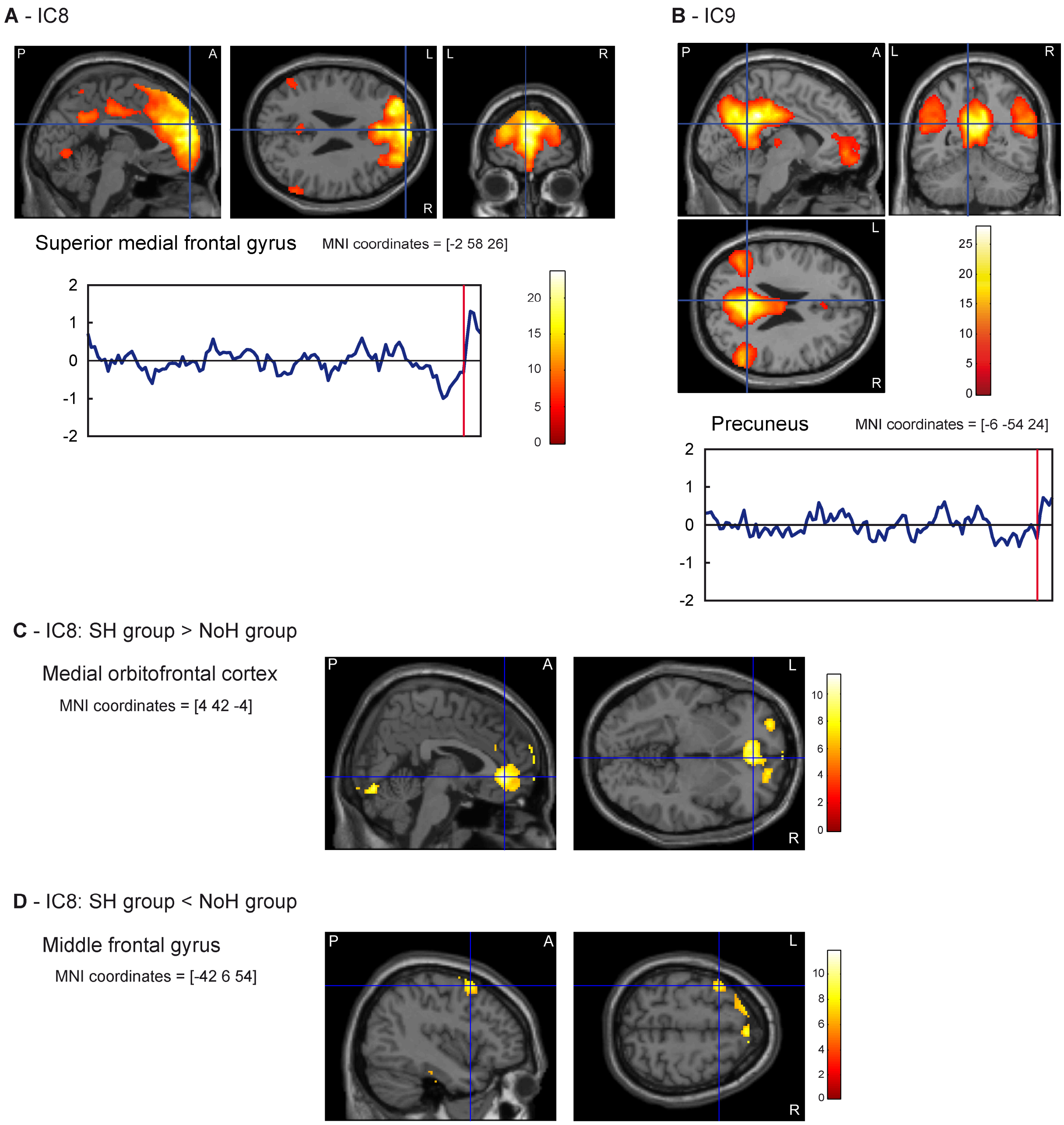

Fig. 5 - Default-mode network. The default-mode network was commonly observed in the two groups and segregated in two independent components. The first is anterior and comprises the medial prefrontal cortex (**A**), whereas the latter includes both the medial and lateral nodes of the posterior default-mode network (**B**). Significant differences between groups in the functional connectivity within this network are shown in panels (**C**) and (**D**). Statistical maps were thresholded at p< 0.05, corrected for family-wise error; the color bars represent *t* values. MNI coordinates (in mm) refer to the crosshair. A = anterior; L = left; P = posterior; R = right.

Supplementary Materials

Table S1 - Subjective rating (VAS) for the three scales evaluating the emotional state of the participants

	Tension		Sadness		Anxiety	
	Pre	Difference Post-Pre	Pre	Difference Post-Pre	Pre	Difference Post-Pre
SH group	-0.3 (2.6)	-1.8 (2.2)	-1.3 (1.2)	-0.5 (1.3)	-1.1 (2.9)	-1.8 (2.8)
NoH group	-1.0 (1.8)	-0.5 (2.4)	-1.3 (1.4)	0.3 (1.9)	-1.5 (2.4)	-0.4 (2.7)

Note. Assessments were performed before and after the experiment, however only the mean ratings reported at the beginning (Pre), and the difference between before and after the experiment (Difference Post-Pre) were computed and reported. SH = Successful Help; NoH = No Help. Standard deviations appear in parentheses.

Table S2 - Mean groups' scores for the four subscales of the Interpersonal Reactivity Index (IRI)

	Fantasy	Empathic concern	Perspective taking	Personal distress
SH group	17.4 (3.4)	19.9 (3.2)	18.0 (4.2)	12.1 (4.1)
NoH group	17.3 (5.5)	18.6 (3.5)	18.6 (3.7)	11.6 (6.1)

Note. SH = Successful Help; NoH = No Help. Standard deviations appear in parentheses.

Table S3 - Mean groups' scores for the five subscales of the Bermond-Vorst Alexithymia Questionnaire (BVAQ-B)

	Verbalizing	Fantasizing	Identifying	Emotionalizing	Analyzing
SH group	2.6 (0.5)	3.1 (0.3)	2.8 (0.6)	3.1 (0.6)	3.1 (0.4)
NoH group	2.8 (0.4)	3.4 (0.3)	2.8 (0.6)	3.0 (0.6)	2.9 (0.6)

Note. SH = Successful Help; NoH = No Help. Standard deviations appear in parentheses.

Table S4 - Mean groups' scores for the three subscales of the Igroup Presence Questionnaire (IPQ) and the general item G

	Involvement	Spatial presence	Experienced realism	General sense of experience
SH group	0.10 (1.3)	0.91 (1.1)	-0.56 (1.2)	1.06 (1.2)
NoH group	0.54 (1.3)	0.68 (1.3)	-0.76 (1.2)	0.11 (1.9)

Note. SH = Successful Help; NoH = No Help. Standard deviations appear in parentheses.

Table S5 - Multivariate tests on self-reported questionnaires and the three scales evaluating the emotional state of the participants

	Wilks λ	*F*	*df*	Error *df*	*p*	η_p^2
Emotional State	0.876	0.658	6	28	0.684	0.124
IRI	0.945	0.436	4	30	0.781	0.055
BVAQ-B	0.816	1.309	5	29	0.288	0.184
IPQ	0.779	2.130	4	30	0.102	0.221

Note. IRI = Interpersonal Reactivity Index; BVAQ-B = Bermond-Vorst Alexithymia Questionnaire, form B; IPQ = Igroup Presence Questionnaire.

Table S6 - Brain regions which were found in Independent Component 1.

Region	Cluster size	x	y	z	Z score
Left precentral gyrus	23115	-30	-4	56	65535
	23115	-34	-12	52	65535
	23115	-26	-18	64	65535
Right precentral gyrus	23115	28	-12	66	65535
	23115	20	-16	64	65535
	23115	20	-28	62	65535
Left postcentral gyrus	23115	-44	-22	50	65535
	23115	-34	-30	58	65535
	23115	-20	-34	68	65535
Right postcentral gyrus	23115	54	-14	46	65535
	23115	32	-34	52	65535
	23115	28	-42	62	65535
Left rolandic operculum	19	-44	-2	10	5.22
	315	-42	-26	16	5.8
	315	-46	-28	16	5.91
Right rolandic operculum	3	46	-20	14	5.13
Left superior frontal gyrus, dorsolateral part	23115	-22	-2	52	65535
Right superior frontal gyrus, dorsolateral part	23115	28	-6	62	65535
Right superior frontal gyrus, medial part	4	8	46	40	5.13
Left middle frontal gyrus	4	-34	40	34	5.02
	23115	-32	10	48	5.56
Right middle frontal gyrus	3	24	32	46	5.12
	23115	30	8	50	5.85
	23115	36	-4	56	65535
Left supplementary motor area	23115	0	-6	56	65535
	23115	-6	-10	64	65535
Right supplementary motor area	23115	12	0	62	65535
	23115	14	-4	52	65535
	23115	4	-6	66	65535
Left paracentral lobule	23115	-16	-14	66	65535
Right paracentral lobule	23115	8	-36	64	7.1
Left median cingulate and paracingulate gyri	23115	-6	22	36	5.33
	23115	-6	-2	42	65535
	23115	-2	-24	48	65535
Right median cingulate and paracingulate gyri	23115	4	10	44	65535
	23115	6	6	42	65535
	23115	2	-28	54	65535
Left insula	315	-38	-20	16	6.19
Left superior parietal gyrus	23115	-22	-48	62	65535
Right superior parietal gyrus	23115	16	-52	60	7.43
	23115	16	-56	58	7.56
Left inferior parietal cortex (except supramarginal and angular gyri)	23115	-30	-46	54	65535

Left precuneus	23115	-18	-40	68	65535
	23115	-12	-48	64	65535
	23115	-14	-60	56	65535
Right precuneus	23115	10	-42	52	7.42
	23115	12	-48	70	7.79
Left superior occipital gyrus	3	-22	-86	26	5.15
Left calcarine fissure and surrounding cortex	1	-8	-60	14	4.94
Right lingual gyrus	1	10	-66	-10	4.91
Left superior temporal gyrus	22	-56	-2	0	5.79
	315	-60	-20	12	6.16
	2	-56	-32	18	5.09
Left temporal pole (superior temporal gyrus)	71	-42	16	-22	5.94
Right temporal pole (superior temporal gyrus)	4	38	26	-30	5.02
Left caudate nucleus	214	-6	4	12	5.46
Right caudate nucleus	18	10	0	14	5.29
Left putamen	1	-30	-18	6	4.92
Left thalamus	214	-8	-6	6	6.31
	214	-14	-14	8	5.79
	214	-20	-22	10	5.36
Left cerebellum, lobules IV and V	318	-4	-56	-2	6.09
Right cerebellum, lobules IV and V	318	8	-40	-8	5.35
	318	8	-48	-10	5.86
	318	8	-50	-6	5.62
Vermis, lobules IV and V	318	2	-50	0	5.84
	318	4	-60	-8	5.07

Note. $p < 0.05$, corrected for multiple comparisons according to the family-wise error approach (FWE-corrected). Coordinates are in millimeters and in the MNI standard space.

Table S7 - Brain regions which were found in Independent Component 2.

Region	Cluster size	x	y	z	Z score
Left precentral gyrus	13545	-34	8	48	7.26
	13545	-36	0	54	65535
	13545	-44	0	44	7.54
Right precentral gyrus	3133	50	6	28	65535
	3133	46	4	44	6.64
	3133	34	2	50	7.64
Right postcentral gyrus	8	54	-14	40	5.12
	10529	52	-24	44	5.34
Left superior frontal gyrus, dorsolateral part	13545	-22	52	8	7.03
	13545	-14	40	32	5.04
	13545	-14	16	46	6.3
Left superior frontal gyrus, medial part	13545	0	32	34	7.59
	13545	2	24	42	65535
	13545	0	18	42	65535
Left superior frontal gyrus, orbital part	13545	-24	58	-4	6.48
	13545	-14	22	-18	6.55
Left middle frontal gyrus	13545	-28	54	16	65535
	13545	-32	52	16	65535
	13545	-22	10	52	65535
Right middle frontal gyrus	3133	40	50	18	6.53
	3133	36	36	28	6.36
	3133	28	6	58	6.75
Left middle frontal gyrus, orbital part	13545	-34	52	-6	5.36
Left inferior frontal gyrus, opercular part	13545	-44	8	30	65535
Right inferior frontal gyrus, opercular part	3133	34	6	30	6.1
Left inferior frontal gyrus, triangular part	13545	-48	22	30	65535
Right inferior frontal gyrus, triangular part	3133	44	32	28	6.19
	3133	46	30	24	6.21
	3133	44	26	24	6.26
Left gyrus rectus	13545	-12	18	-12	6.86
Right gyrus rectus	295	12	20	-12	5.31
Left supplementary motor area	13545	-2	20	56	7.26
	13545	-4	10	50	65535
	13545	0	4	52	65535
Left anterior cingulate and paracingulate gyri	13545	-8	36	22	6.66
	13545	-4	30	30	7.41
Right anterior cingulate and paracingulate gyri	13545	8	32	14	65535
	13545	6	16	26	65535
	13545	2	10	28	7.75
Left median cingulate and paracingulate gyri	13545	-4	22	36	7.84
	10529	-8	-34	42	6.32
	10529	-6	-42	46	6.99

Right median cingulate and paracingulate gyri	13545	4	14	46	65535
	13545	8	14	42	65535
Right median cingulate and paracingulate gyri	4	2	-16	46	5.11
Left insula	13545	-28	22	-8	6.6
	13545	-36	20	4	5.92
Right superior parietal gyrus	10529	20	-62	50	6.9
Left inferior parietal cortex (except supramarginal and angular gyri)	10529	-42	-36	40	65535
	10529	-36	-58	50	65535
	10529	-28	-60	42	65535
Right inferior parietal cortex (except supramarginal and angular gyri)	10529	32	-50	44	65535
Right angular gyrus	10529	34	-56	50	65535
	10529	32	-60	40	7.65
Right supramarginal gyrus	10529	50	-30	46	5.83
Left precuneus	10529	-10	-54	46	6.9
	10529	-8	-64	48	65535
	10529	-12	-74	46	65535
Right precuneus	10529	4	-54	46	6.82
	10529	8	-56	46	6.8
	10529	16	-64	48	7.18
Left superior occipital gyrus	10529	-26	-70	34	65535
Right superior occipital gyrus	10529	30	-64	42	7.58
	10529	32	-70	42	7.66
Left middle occipital gyrus	10529	-28	-78	34	65535
	10529	-38	-82	26	6.81
	10529	-38	-88	-2	6.69
Right middle occipital gyrus	10529	34	-74	36	7.55
	10529	44	-78	28	5.89
	1	48	-80	0	4.92
Left inferior occipital gyrus	10529	-48	-66	-16	7.54
	10529	-48	-76	-2	6.26
	10529	-46	-78	-6	6.31
Left cuneus	10529	-14	-72	32	6.02
Left calcarine fissure and surrounding cortex	19	-16	-60	16	5.25
Right calcarine fissure and surrounding cortex	6	14	-56	12	5.06
	14	8	-78	10	5.45
Left lingual gyrus	361	-10	-44	0	6.07
Right lingual gyrus	12	10	-44	6	5.4
Left fusiform gyrus	10529	-36	-40	-24	5.98
Left superior temporal gyrus	372	-66	-18	4	5.72
	372	-54	-18	2	6.77
Right superior temporal gyrus	24	62	-12	-2	5.68
Left middle temporal gyrus	372	-54	-16	-4	6.35
	372	-64	-26	0	6.08
	111	-58	-48	8	6.09

Left inferior temporal gyrus	10529	-56	-58	-8	6.12
Left olfactory cortex	13545	-8	12	-12	6.56
Left temporal pole (superior temporal gyrus)	22	-48	16	-16	5.29
Left temporal pole (middle temporal gyrus)	3	-28	12	-34	4.95
Left caudate nucleus	13545	-8	18	6	5.91
Right caudate nucleus	295	8	16	-10	5.17
	295	8	8	4	7.1
Left putamen	13545	-28	14	2	5.73
	13545	-18	12	2	5.64
Right putamen	295	22	18	-8	6.19
Left globus pallidus	13545	-10	4	2	5.54
Left thalamus	1	-8	-18	8	5.17
Left cerebellum, lobule VI	10529	-42	-48	-26	6.57

Note. $p < 0.05$, corrected for multiple comparisons according to the family-wise error approach (FWE-corrected). Coordinates are in millimeters and in the MNI standard space.

Table S8 - Brain regions which were found in Independent Component 3.

Region	Cluster size	x	y	z	Z score
Right superior frontal gyrus, dorsolateral part	10228	32	56	12	65535
	10228	18	30	46	65535
	10228	20	26	50	65535
Left superior frontal gyrus, medial part	10228	2	34	40	65535
Right superior frontal gyrus, medial part	10228	12	36	48	65535
Right superior frontal gyrus, medial orbital part	1	8	50	-6	4.95
Left middle frontal gyrus	105	-42	56	4	5.27
	30	-40	20	40	5.26
	73	-28	10	56	6.4
Right middle frontal gyrus	10228	28	26	48	65535
	10228	46	22	40	65535
	10228	38	10	56	65535
Left middle frontal gyrus, orbital part	105	-32	50	-8	5.02
	105	-42	48	-8	5.91
Right middle frontal gyrus, orbital part	10228	30	58	-6	65535
	10228	42	50	-8	65535
	10228	46	48	-14	7.8
Right inferior frontal gyrus, opercular part	10228	54	20	4	5.44
Right inferior frontal gyrus, triangular part	10228	48	36	18	65535
	10228	50	30	30	65535
	10228	58	22	16	6.3
Right inferior frontal gyrus, orbital part	10228	46	44	-8	7.51
	10228	32	42	-18	7.38
	10228	40	40	-2	7.09
Right anterior cingulate and paracingulate gyri	10228	6	46	6	7.19
	10228	6	40	28	65535
	537	6	-34	38	7.6
Right insula	10228	34	16	-14	5.09
	1	34	-16	10	5.03
Left inferior parietal cortex (except supramarginal and angular gyri)	782	-50	-46	48	7.55
	782	-44	-56	48	6.41
	782	-38	-62	52	5.83
Right inferior parietal cortex (except supramarginal and angular gyri)	4438	44	-46	52	65535
	4438	46	-46	46	65535
	4438	42	-56	44	65535
Left angular gyrus	782	-48	-62	50	6.35
Right angular gyrus	4438	56	-52	38	65535
	4438	48	-52	30	65535
	4438	56	-54	30	65535
Right supramarginal gyrus	4438	56	-44	44	65535

Right precuneus	537	6	-58	42	6.62
	18	8	-66	32	4.92
	19	6	-78	50	5.35
Right cuneus	2	14	-62	22	4.92
	18	8	-68	24	5.26
Right superior temporal gyrus	109	46	-4	-8	5.64
	109	46	-6	-12	5.6
Right inferior temporal gyrus	787	66	-30	-18	6.4
	787	64	-40	-10	65535
Right temporal pole (superior temporal gyrus)	1	30	26	-30	5.17
Right parahippocampal gyrus	1	22	16	-30	5.05
Vermis, lobules IV and V	3	4	-46	-6	5.01
	1	0	-46	-12	4.98

Note. $p < 0.05$, corrected for multiple comparisons according to the family-wise error approach (FWE-corrected). Coordinates are in millimeters and in the MNI standard space.

Table S9 - Brain regions which were found in Independent Component 4.

Region	Cluster size	x	y	z	Z score
Right precentral gyrus	92	54	-2	48	5.93
Left postcentral gyrus	59	-54	-12	46	6.19
	45	-40	-14	36	5.6
	9	-22	-28	60	5.21
Right postcentral gyrus	7947	58	-6	28	5.6
Left rolandic operculum	9012	-60	-2	12	7.05
Left middle frontal gyrus	6	-26	46	26	5.35
Left inferior frontal gyrus, triangular part	233	-40	16	26	6.82
Left gyrus rectus	35	-10	54	-16	4.97
	35	0	52	-20	5.64
Right median cingulate and paracingulate gyri	491	10	-38	52	5.09
Left insula	9012	-40	-2	10	6.08
Left precuneus	491	-2	-52	46	6.99
Right precuneus	1	8	-56	22	4.92
Right calcarine fissure and surrounding cortex	54	12	-86	10	5.61
	54	8	-90	12	4.97
Left superior temporal gyrus	9012	-60	4	-8	65535
	9012	-42	-30	8	65535
	9012	-66	-38	12	65535
Right superior temporal gyrus	7947	58	0	-8	65535
	7947	48	-14	0	65535
	7947	62	-16	4	65535
Left rolandic operculum (Heschl gyrus)	9012	-46	-18	8	65535
Right rolandic operculum (Heschl gyrus)	7947	44	-20	6	65535
Left middle temporal gyrus	9012	-58	-4	-16	65535
	9012	-56	-28	4	65535
	9012	-56	-48	12	7.65
Right middle temporal gyrus	7947	56	-2	-14	65535
	7947	64	-4	-10	65535
	7947	66	-14	-10	65535
Left temporal pole (superior temporal gyrus)	9012	-54	8	-10	65535
Right temporal pole (superior temporal gyrus)	7947	54	10	-12	65535
Left cerebellum. lobules IV and V	4	-6	-48	-18	5.02
Vermis, lobules IV and V	1	-2	-52	-10	5.02
	1	0	-54	-8	4.97

Note. $p < 0.05$, corrected for multiple comparisons according to the family-wise error approach (FWE-corrected). Coordinates are in millimeters and in the MNI standard space.

Table S10 - Brain regions which were found in Independent Component 5.

Region	Cluster size	x	y	z	Z score
Right middle frontal gyrus	1	40	44	10	4.97
Right supplementary motor area	2	4	20	62	5.06
Left precuneus	38	-4	-50	46	5.6
	38	-10	-52	42	5.05
Left cuneus	6636	-8	-78	34	65535
	6636	4	-90	18	65535
	6636	-6	-94	18	65535
Right cuneus	6636	4	-80	26	65535
	6636	14	-90	24	65535
Left calcarine fissure and surrounding cortex	6636	-6	-94	6	65535
Right calcarine fissure and surrounding cortex	6636	6	-82	10	65535
	6636	8	-90	4	65535

Note. $p < 0.05$, corrected for multiple comparisons according to the family-wise error approach (FWE-corrected). Coordinates are in millimeters and in the MNI standard space.

Table S11 - Brain regions which were found in Independent Component 6.

Region	Cluster size	x	y	z	Z score
Right precentral gyrus	503	40	-18	62	5.83
	503	38	-20	54	5.72
Left postcentral gyrus	87	-42	-32	58	5.47
	87	-40	-32	48	5.86
	87	-36	-32	46	5.67
Right postcentral gyrus	503	56	-18	52	6.74
	503	56	-24	54	6.67
	503	48	-26	56	7.6
Right superior frontal gyrus, dorsolateral part	1	18	66	14	5.01
Left superior frontal gyrus, medial part	372	-2	58	34	5.47
Right superior frontal gyrus, medial part	372	4	70	8	7.17
	372	4	66	20	6.05
	372	4	64	28	5.84
Left superior parietal gyrus	14987	-26	-66	48	6.51
Left inferior parietal cortex (except supramarginal and angular gyri)	7	-56	-20	50	5.13
Right inferior parietal cortex (except supramarginal and angular gyri)	14987	28	-54	54	5.1
Right angular gyrus	14987	26	-58	44	5.81
	14987	26	-62	48	5.89
Left precuneus	7	-4	-50	18	5
Right precuneus	60	18	-50	20	6.32
Left superior occipital gyrus	14987	-26	-68	32	6.24
	14987	-14	-96	8	65535
Right superior occipital gyrus	14987	28	-64	34	5.26
Left middle occipital gyrus	14987	-42	-80	2	65535
	14987	-32	-92	8	65535
	14987	-18	-102	6	65535
Right middle occipital gyrus	14987	36	-84	6	65535
	14987	40	-88	2	65535
	14987	34	-96	0	65535
Left inferior occipital gyrus	14987	-48	-66	-12	65535
	14987	-44	-78	-4	65535
Right inferior occipital gyrus	14987	42	-68	-10	65535
	14987	44	-76	-6	65535
	14987	36	-82	-6	7.67
Left calcarine fissure and surrounding cortex	14987	-4	-82	-8	65535
	14987	4	-86	0	65535
	14987	4	-96	0	65535
Right calcarine fissure and surrounding cortex	14987	6	-92	10	65535
	14987	16	-96	2	65535
Left lingual gyrus	14987	-28	-82	-12	65535

Right lingual gyrus	14987	8	-78	-4	65535
	14987	16	-88	-4	65535
	14987	10	-90	-4	65535
Left fusiform gyrus	14987	-30	-62	-16	65535
	14987	-28	-66	-12	7.8
	14987	-24	-82	-10	65535
Right fusiform gyrus	14987	34	-56	-12	65535
	14987	32	-64	-12	65535
	14987	28	-70	-10	65535
Right inferior temporal gyrus	14987	50	-42	-20	6.4
	14987	50	-64	-10	7.14
	14987	44	-72	-8	65535
Left hippocampus	17	-24	-6	-22	5.48
Left thalamus	83	-14	-16	8	5.51
Right thalamus	1	10	-8	2	5.01
Left cerebellum, lobules IV and V	14987	-22	-50	-16	7.23
Left cerebellum, lobule VI	14987	-40	-54	-22	65535
	14987	-18	-68	-16	7.16
Vermis, lobules VI	14987	-2	-64	-16	5.16

Note. $p < 0.05$, corrected for multiple comparisons according to the family-wise error approach (FWE-corrected). Coordinates are in millimeters and in the MNI standard space.

Table S12 - Brain regions which were found in Independent Component 7.

Region	Cluster size	x	y	z	Z score
Left rolandic operculum	27	-42	-24	18	5.59
Right rolandic operculum	3488	56	14	0	65535
Right superior frontal gyrus, medial part	3492	6	60	4	5.23
Right superior frontal gyrus, medial orbital part	3492	6	60	-2	4.95
Left inferior frontal gyrus, orbital part	3608	-46	16	-4	65535
Right inferior frontal gyrus, orbital part	3488	52	28	-2	65535
	3488	34	26	-10	65535
	3488	38	22	-18	65535
Left supplementary motor area	3492	-2	12	60	5.69
	3492	-4	12	56	5.68
Right supplementary motor area	2	6	22	52	4.94
Left anterior cingulate and paracingulate gyri	3492	-6	44	6	7.64
	3492	-4	38	18	7.75
	3492	-2	32	26	65535
Right anterior cingulate and paracingulate gyri	3492	6	48	4	7.47
	3492	4	40	12	7.81
	3492	2	34	22	7.78
Left median cingulate and paracingulate gyri	3492	0	20	36	7.54
Right median cingulate and paracingulate gyri	3492	6	10	44	6.24
Left insula	3608	-34	22	-8	65535
	3608	-36	20	-12	65535
	3608	-42	10	-4	65535
Right insula	3488	34	18	2	65535
	3488	42	8	0	6.86
	13	32	-18	12	5.75
Right angular gyrus	248	58	-50	28	5.95
	248	56	-54	38	5.53
Left supramarginal gyrus	3	-60	-46	28	5.08
Right supramarginal gyrus	248	62	-40	34	6.2
	248	60	-44	32	5.95
	248	64	-44	30	6.33
Left precuneus	22	-4	-62	64	5.45
Right middle temporal gyrus	130	62	-22	-14	5.88
	130	52	-30	-8	5.76
Right inferior temporal gyrus	130	60	-22	-18	5.58
Left temporal pole (superior temporal gyrus)	3608	-42	18	-14	65535
	3608	-32	18	-30	6.82
Right temporal pole (superior temporal gyrus)	3488	50	18	-10	65535
	3488	52	8	-4	7.6
Left putamen	3608	-30	4	-6	7.14
	3	-28	-12	10	5.11
Right putamen	4	22	12	-4	5.06

Left thalamus	1961	-16	-14	6	6.56
	1961	-6	-16	0	65535
Right thalamus	1961	6	-14	8	7.19
	1961	6	-20	0	65535
	1961	10	-28	0	6.73
Right cerebellum, lobules IV and V	357	16	-50	-20	6.79
Left cerebellum, lobule VI	39	-36	-54	-26	5.27
	39	-30	-56	-24	5.07
	39	-24	-60	-20	5.6
Right cerebellum, lobule VI	357	10	-60	-16	6.99
Vermis, lobules IV and V	357	0	-54	-18	5.95

Note. $p < 0.05$, corrected for multiple comparisons according to the family-wise error approach (FWE-corrected). Coordinates are in millimeters and in the MNI standard space.

1 Table S13 - Brain regions which were found in Independent Component 8.

Region	Cluster size	x	y	z	Z score
Right precentral gyrus	36	22	-30	68	5.63
Left postcentral gyrus	3	-50	-12	38	5.17
Right postcentral gyrus	25	50	-4	32	5.21
Right postcentral gyrus	25	54	-6	34	5.35
Left superior frontal gyrus, dorsolateral part	16528	-24	58	18	65535
	16528	-20	46	24	65535
	16528	-14	24	58	65535
Right superior frontal gyrus, dorsolateral part	16528	18	56	30	65535
	16528	16	52	32	65535
	16528	16	42	50	65535
Left superior frontal gyrus, medial part	16528	-2	58	24	65535
	16528	-8	50	42	65535
	16528	-8	42	44	65535
Right superior frontal gyrus, medial part	16528	2	58	8	65535
	16528	4	52	40	65535
	16528	4	46	50	65535
Left middle frontal gyrus	16528	-32	48	24	65535
	16528	-28	34	44	65535
	16528	-24	30	50	65535
Right middle frontal gyrus	16528	26	52	26	65535
	16528	24	46	34	65535
	16528	30	34	38	65535
Left gyrus rectus	16528	0	58	-16	7.01
Left supplementary motor area	16528	0	22	62	7.49
	16528	-2	16	64	7.32
Right supplementary motor area	6	12	4	64	5.09
	11	4	-14	70	5.15
Left anterior cingulate and paracingulate gyri	16528	-2	48	10	65535
	16528	2	46	18	65535
	16528	-4	30	28	65535
Right anterior cingulate and paracingulate gyri	16528	2	40	20	65535
Left median cingulate and paracingulate gyri	16528	-2	6	40	5.04
	16528	0	-16	40	6.89
Right median cingulate and paracingulate gyri	16528	2	24	38	7.45
	16528	10	24	34	7.01
	16528	2	-26	42	7.55
Left posterior cingulate gyrus	377	-4	-46	34	6.76
Right inferior parietal cortex (except supramarginal and angular gyri)	221	58	-58	40	6.17
Left angular gyrus	163	-48	-58	32	6.09
	163	-52	-62	34	5.68
Right angular gyrus	221	52	-54	32	5.56
Left precuneus	377	-2	-54	32	6.76
Right precuneus	42	2	-54	60	6.18

Right superior occipital gyrus	14	22	-84	38	5.59
	139	24	-84	18	5.11
	139	24	-94	20	5.09
Right middle occipital gyrus	139	40	-84	16	5.39
	139	30	-88	20	5.88
Left lingual gyrus	170	-6	-74	-2	5.6
Left middle temporal gyrus	24	-66	-20	-14	5.16
	24	-66	-22	-10	5.12
	23	-58	-26	-2	5.64
Left inferior temporal gyrus	9	-38	14	-38	5.29
	3	-46	6	-32	5.01
	73	-64	-16	-26	6.34
Left temporal pole (superior temporal gyrus)	18	-50	18	-10	5.53
Right caudate nucleus	86	16	16	12	5.93

Note. $p < 0.05$, corrected for multiple comparisons according to the family-wise error approach (FWE-corrected). Coordinates are in millimeters and in the MNI standard space.

Table S14 - Brain regions which were found in Independent Component 9.

Region	Cluster size	x	y	z	Z score
Right postcentral gyrus	134	46	-22	60	5.84
	134	48	-24	54	6.02
Left superior frontal gyrus, dorsolateral part	137	-22	60	10	6.05
Left superior frontal gyrus, medial part	137	-12	66	14	5.47
Right superior frontal gyrus, medial part	2138	6	56	6	7.11
	2138	4	54	16	6.2
	2138	2	54	8	6.98
Left superior frontal gyrus, orbital part	137	-22	60	-4	5.82
Left superior frontal gyrus, medial orbital part	2138	0	56	-8	7.21
	2138	-6	50	-6	7.61
Right superior frontal gyrus, medial orbital part	2138	4	62	-2	7.02
	2138	2	60	-12	7.27
	2138	4	52	-12	7.3
Left middle frontal gyrus	2	-22	34	44	4.96
	2	-28	22	50	4.98
	1	-30	20	52	4.94
Left gyrus rectus	2138	-2	58	-14	7.27
Left anterior cingulate and paracingulate gyri	2138	0	42	12	6.71
	2138	0	32	18	6.27
Right anterior cingulate and paracingulate gyri	2138	4	48	16	6.36
	2138	4	44	14	6.48
Left median cingulate and paracingulate gyri	8842	0	-22	34	65535
	8842	-6	-32	40	65535
Right median cingulate and paracingulate gyri	8842	6	-46	34	65535
Left posterior cingulate gyrus	8842	-6	-42	32	65535
	8842	-4	-48	28	65535
Left inferior parietal cortex (except supramarginal and angular gyri)	2870	-50	-44	42	5.85
Left angular gyrus	2870	-44	-60	30	65535
	2870	-40	-64	40	65535
	2870	-46	-64	32	65535
Right angular gyrus	2478	56	-60	28	65535
	2478	42	-64	38	65535
	2478	44	-66	46	65535
Left precuneus	8842	-6	-54	22	65535
	8842	0	-62	22	65535
	8842	-4	-66	34	65535
Right precuneus	8842	4	-52	22	65535
	8842	8	-56	28	65535
Right inferior occipital gyrus	6	32	-90	-4	5.28
Left middle temporal gyrus	29	-66	-42	-10	5.37

Right middle temporal gyrus	12	64	-12	-22	5.53
	126	66	-30	-6	6.06
	126	62	-32	-6	5.76
Left parahippocampal gyrus	59	-26	-22	-20	6.07
Left thalamus	42	-6	-22	6	5.93
Vermis, lobules IV and V	8842	-6	-46	4	7.73

Note. $p < 0.05$, corrected for multiple comparisons according to the family-wise error approach (FWE-corrected). Coordinates are in millimeters and in the MNI standard space.

Table S15 - Brain regions of IC 7 which were found significant in the contrast SH group < NoH group

Region	Cluster size	x	y	z	Z score
Left superior frontal gyrus, dorsolateral part	18	-16	42	30	5,19
	408	-12	22	48	6,16
Right superior frontal gyrus, dorsolateral part	4	24	32	56	5,17
	11	20	28	48	5,1
	11	16	26	46	5,13
	5	14	16	50	5,18
Left superior frontal gyrus, medial part	18	-10	46	34	5,37
	408	-4	36	52	5,89
	408	-8	26	44	5,37
Right superior frontal gyrus, medial part	408	4	42	44	5,77
	11	12	28	46	5,13
Right middle frontal gyrus	12	40	14	58	5,88
Right inferior frontal gyrus, orbital part	122	36	24	-16	6,41
Left supplementary motor area	408	-10	18	58	5,41
Left anterior cingulate and paracingulate gyri	28	-8	36	20	5,8
	408	-2	22	38	5,67
Right median cingulate and paracingulate gyri	4	8	20	38	4,99
Left insula	142	-40	20	-4	5,25
	142	-32	20	-12	5,38
	142	-36	18	-2	5,27
	142	-44	18	-2	5,71
	142	-46	16	2	5,72
Right insula	1	36	12	-6	5,09
	9	46	-4	4	5,34
Right superior parietal gyrus	1	34	-74	54	5,16
Right angular gyrus	20	50	-66	48	5,3
	20	42	-68	54	5,22
	20	38	-74	52	5,39
Left middle occipital gyrus	2	-18	-92	6	5,08
Right superior temporal gyrus	7	56	-14	-6	5,24
Left putamen	38	-28	6	-2	5,65

Note. $p < 0.05$, corrected for multiple comparisons according to the family-wise error approach (FWE-corrected). Coordinates are in millimeters and in the MNI standard space.

Table S16 - Brain regions of IC 7 which were found significant in the contrast SH group > NoH group

Region	Cluster size	x	y	z	Z score
Left precentral gyrus	38	-60	8	38	6,52
	38	-58	2	44	6,34
	1	-54	-2	52	5,45
Left postcentral gyrus	38	-58	-2	46	6,24
	38	-60	-2	42	5,89
Right postcentral gyrus	597	54	-20	36	5,94
Right rolandic operculum	597	62	-18	16	5,85
Left middle frontal gyrus	212	-26	56	34	6,03
	212	-46	44	28	7,69
	212	-44	38	38	7,35
Right middle frontal gyrus	2	30	52	36	5,07
	285	44	52	14	6,42
	285	46	48	22	6,27
Right inferior frontal gyrus, triangular part	285	52	44	4	5,32
	285	52	42	8	5,32
	285	56	38	6	5,48
Left inferior parietal cortex (except supramarginal and angular gyri)	1	-56	-38	48	4,97
Left supramarginal gyrus	172	-60	-26	38	5,98
	172	-54	-26	32	5,4
	172	-50	-32	36	5,04
Right supramarginal gyrus	597	66	-18	30	5,83
	597	68	-24	30	5,88
	597	66	-30	28	5,97
Right superior occipital gyrus	6	22	-76	40	5,31
Left middle occipital gyrus	1	-34	-66	40	4,94
Right inferior occipital gyrus	2967	46	-72	-14	7,01
Right fusiform gyrus	2967	30	-74	-16	6,66
Left superior temporal gyrus	172	-58	-30	24	5,27
Right superior temporal gyrus	597	68	-26	16	5,6
	597	64	-32	18	5,95
Left middle temporal gyrus	2	-56	-64	-2	5,08
Right inferior temporal gyrus	2967	62	-58	-8	5,34
	2967	56	-66	-12	6,1
Right temporal pole (superior temporal gyrus)	2	22	16	-32	5,47

Note. $p < 0.05$, corrected for multiple comparisons according to the family-wise error approach (FWE-corrected). Coordinates are in millimeters and in the MNI standard space.

Table S17 - Brain regions of IC 8 which were found significant in the contrast SH group > NoH group

Region	Cluster size	x	y	z	Z score
Right rolandic operculum	1	52	2	6	5
	2	50	0	12	5,07
	1	38	-20	18	4,96
Left superior frontal gyrus, dorsolateral part	96	-22	68	10	7,19
	96	-28	62	18	6,18
Right superior frontal gyrus, dorsolateral part	1	16	68	12	5,01
	2	16	62	26	5,02
	1241	18	56	2	5,92
Left superior frontal gyrus, medial part	141	-2	70	12	6,59
	141	0	66	22	6,9
	6	-12	56	16	5,04
Right superior frontal gyrus, medial part	141	10	72	8	5,7
	141	10	68	18	5,84
	1241	10	60	4	5,4
Left superior frontal gyrus, orbital part	52	-26	58	-4	5,96
Left superior frontal gyrus, medial orbital part	1	-14	60	-2	4,97
	1241	-10	44	-8	6,22
Right superior frontal gyrus, medial orbital part	1241	4	56	-10	5,27
	1241	4	42	-4	7,08
Right middle frontal gyrus	3	32	54	30	5,1
	1	36	46	8	4,96
Right inferior frontal gyrus, triangular part	55	42	32	2	5,01
	55	46	28	6	5,4
	55	50	22	2	5,85
Left gyrus rectus	1241	-6	34	-20	5,04
Right gyrus rectus	1241	6	48	-14	5,57
Left anterior cingulate and paracingulate gyri	1241	-4	44	10	5,8
	1241	-6	40	-6	6,57
	10	-8	24	26	5,33
Right anterior cingulate and paracingulate gyri	8	4	34	22	5,16
Left median cingulate and paracingulate gyri	4	-8	14	36	5,22
Left insula	4	-34	18	4	5,13
Right insula	31	36	28	2	5,11
Right precuneus	108	10	-66	30	6,39
Left cuneus	78	-8	-72	28	5,68
Right inferior temporal gyrus	3	32	8	-42	5,23
	20	48	6	-34	6,38
	4	48	-2	-40	5,46
Left caudate nucleus	11	-16	20	6	5,42
Right caudate nucleus	2	14	22	10	5,01
	9	10	20	12	5,22

Note. $p < 0.05$, corrected for multiple comparisons according to the family-wise error approach (FWE-corrected). Coordinates are in millimeters and in the MNI standard space.

Table S18 - Brain regions of IC 8 which were found significant in the contrast SH group < NoH group

Region	Cluster size	x	y	z	Z score
Left precentral gyrus	290	-54	12	42	6,31
	290	-46	8	50	6,36
	3	-42	0	64	5,47
Left superior frontal gyrus, dorsolateral part	1	-14	54	44	5,05
	344	-16	42	54	6,22
	344	-16	28	62	5,45
Left superior frontal gyrus, medial part	27	2	56	40	5,22
	344	-6	26	62	5,3
Right superior frontal gyrus, medial part	27	2	52	46	5,13
	344	4	34	60	6,98
	344	4	26	62	6,02
Right superior frontal gyrus, orbital part	33	16	32	-22	5,3
	33	12	26	-22	5,49
Left middle frontal gyrus	1	-50	32	34	5,09
	290	-40	10	58	6,09
	290	-38	8	62	6,04
Right middle frontal gyrus	7	48	46	20	5,13
	7	52	44	16	5,24
Right middle frontal gyrus, orbital part	57	46	52	-14	7,35
Left inferior frontal gyrus, triangular part	2	-52	30	32	5,51
	1	-54	28	30	5,26
Left supplementary motor area	344	-10	18	64	5,69
	344	-10	12	66	5,52
	344	-4	10	68	5,01
Right supplementary motor area	344	4	18	64	6,32
Left inferior temporal gyrus	7	-42	-26	-20	5,22
	1	-52	-34	-26	5,12

Note. $p < 0.05$, corrected for multiple comparisons according to the family-wise error approach (FWE-corrected). Coordinates are in millimeters and in the MNI standard space.

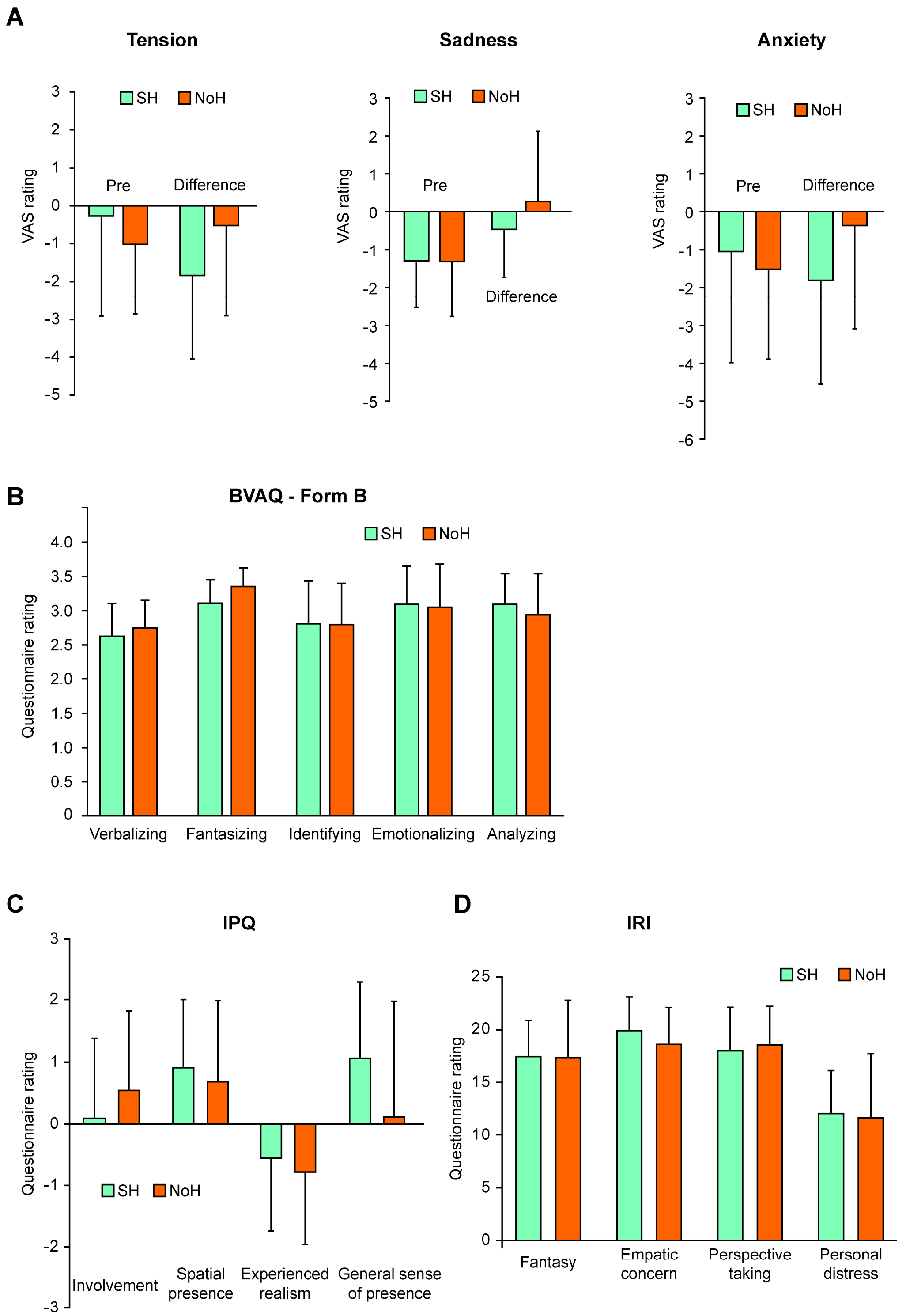

Fig. S1 - Results of behavioral surveys and questionnaires. Mean groups' scores for the three scales evaluating the emotional state (Tension, Sadness, and Anxiety - **A**) of the participants, the Bermond-Vorst Alexithymia Questionnaire, form B (BVAQ-B - **B**), the Igroup Presence Questionnaire (IPQ - **C**), and the Interpersonal Reactivity Index (IRI - **D**). Error bars represent standard deviations.